medium (YPD) and synthetic complete medium (using Difco yeast nitrogen base) lacking leucine (SC-Leu), lacking uracil (SC-Ura), and lacking leucine and uracil (SC-Leu-Ura) were used (Sherman 2002). SRaf-Leu and SRaf-Leu-Ura media contained 2% raffinose instead of glucose. To induce expression of the *GAL1* and *CUP1* promoters, galactose and $CuSO_4$ were added to final concentrations of 2% and 50 μM, respectively. Yeast strains were grown at 30 °C.

Plasmids

The yeast plasmid YCp-GAL1p-SUP35 (NM)–GFP [*LEU2*], expressing the Sup35NM domain conjugated to GFP by the galactose inducible *GAL1* promoter, was previously described (Ayano *et al.* 2004). To analyze nonsense suppression at a single-cell level, the yeast plasmid YCp-CUP1-NLS-mRFP [*URA3*] containing nonsense mutations was constructed. To construct YCp-CUP1-NLS-mRFP, we introduced nonsense mutations into pRSET-B-mRFP (a gift from Dr Roger Tsien) with the QuikChange™ Site-directed Mutagenesis Kit (Stratagene) using the two sets of primer pairs: mRFP-ochre-F, GAGGACGTCATCAAGTAATTCATGCGCTTCAAG, mRFP-ochre-R, CTTGAAGCGCATGAATTACTTGATGACGTCCTC and mRFP-opal-F, GAGGACGTCATCAAGTGATTCATGCGCTTCAAG, mRFP-opal-R, CTTGAAGCGCATGAATCACTTGATGACGTCCTC and mRFP-amber-F, GAGGACGTCATCAAGTAGTTCATGCGCTTCAAG, mRFP-amber-R, CTTGAAGCGCATGAACTACTTGATGACGTCCTC (underlines are nonsense mutations), and digested them with *Bam*HI and *Eco*RI. The resulting *Bam*HI-*Eco*RI fragments were inserted into the yeast plasmid YCp-CUP1p (King 2001) digested with *Bam*HI and *Eco*RI (YCp-CUP1p-mRFP). The NLS (Nuclear location signal) sequence amplified from the yeast plasmid pYO2568 (a gift from Dr Yoshikazu Ohya) with the two sets of primer pairs: F-BamHINLSGAP, CGCGGATCCATGGATAAAGC and R-BamHINLSGAD, GCGGGATCCCTCTTTTTTTTG was digested with *Bam*HI, and inserted into YCp-CUP1p-mRFP. The yeast plasmid YCp-CUP1p-SUP35 (NM)–GFP [*URA3*], expressing Sup35NM-GFP from a copper inducible *CUP1* promoter, is described below. The NM domain region of the entire *SUP35* ORF was amplified with primers GCGGGATCCACAATGTCGGATTCAAACCA and CCGGCCGAGCTCTATCGTTAACAAC. The PCR products were digested with *Bam*HI and *Sac*I and inserted into YCp-CUP1p. The GFP fragment was amplified with primers CCGAGCTCCCATGGCTAGCAAAGGAGAAGAA and CCGGCCGAATTCCCACCGCTGCCATG, digested with *Sac*I and *Eco*RI, and inserted into YCp-CUP1p-SUP35NM.

Single-cell imaging

The on-chip microculture system (Supplementary Fig. 1A) is the same as that previously described (Ayano *et al.* 2004), except for the microchamber design (Supplementary Fig. S1B), which was designed for long-term cultivation of individual, isolated yeast cells and for efficient exchange of fresh medium. The microculti-vation chamber array chip consisted of microchambers positioned on 0.2-mm-thick glass slides. By enclosing the cells in the microchambers, we were able to observe them in liquid medium for a long time without them leaving the field of vision of the objective lens (Inoue *et al.* 2001a; Umehara *et al.* 2003; Ayano *et al.* 2004). The microchamber array, which was made of negative photoresist SU-8 10 (Microlithography Chemical Co. Newton, MA, USA), was photolighographically microfabricated on a glass slide (Ayano *et al.* 2004). Each microchamber in the array was designed with a surface area of 1500 μm^2 and a 10-μm-high wall. The cultivation system was used with a bright-field optical microscopy system (IX-70 inverted microscopy with a 100× objective lens, Olympus) with a cooled CCD camera (ORCA II-ER, Hamamatsu Photonics) to obtain phase contrast (or differential interference contrast) and fluorescent images. A 10 μL aliquot of a 1 mg/mL bovine serum albumin solution was spread on the microchamber array plate, to prevent the cells from adhering to the microchamber surface. After a 10 min incubation, 10 μL of a mid-log phase yeast culture was dispensed on to the microchamber array plate. The cover was then placed on the microchamber array plate and sealed with polydimethylsiloxane (Dow Corning, Midland, MI, USA). The covered chamber was then connected to the medium tanks and positioned on the stage of the microscope.

During on-chip cultivation, fresh medium was continuously supplied to the chamber system at constant rate of 1 mL/min by a peristaltic pump. A syringe was used for the immediate exchange of medium. Yeast cells were grown in SC-Leu. To induce the expression of Sup35NM-GFP, 2% galactose was used instead of 2% glucose in synthetic medium (SGal-Leu). To stop yeast growth, an isotonic nutrient-free buffer (10 mM potassium phosphate, pH 7.0 and 1.2 M sorbitol) was used. The temperature of the system was maintained at 30 °C throughout the observations by a heated chamber surrounding the microscope.

Nonsense suppressor analysis

For the conventional nonsense suppressor analysis, yeast cells with or without Sup35-GFP foci were plated on SC-Leu and SC-Leu-Ade for 3 days (Serio *et al.* 1999). For the single-cell translational read-through assay, [*PSI*$^+$] cells bearing Sup35-GFP foci were transferred to a culture without the inducer ($CuSO_4$). After the disappearance of the GFP-Sup35 foci, NLS-mRFP containing a nonsense mutation (from the YCp-CUP1p-NLS-mRFP plasmid) was induced by adding 50 mM $CuSO_4$. The appearance of mRFP in the nucleus was observed by fluorescence microscopy (IX-71 inverted microscope with an objective lens, ×100, Olympus) at 10 h postinduction.

Cell lysis

Yeast strains containing YCp-GAL1p-SUP35(NM)–GFP were grown to mid-log phase in SRaf-Leu. After 2% galactose was added, the yeast were incubated for 4 h at 30 °C. Cells were collected by centrifugation, broken with glass beads (Sigma) by vortexing for 1 min at 4 °C in lysis buffer (50 mM Tris-HCl, pH 7.5, 5 mM $MgCl_2$, 10 mM KCl, 0.1 mM EDTA, pH 8.0,

1 mM DTT, Complete™ protease inhibitor cocktail EDTA-free (Roche)), and incubated for 2 min on ice. This procedure was repeated for 4–6 cycles. The crude lysates were clarified by centrifugation.

Semi-denaturing agarose gel electrophoresis

Yeast lysates were incubated in sample buffer (0.5×TAE, 2% SDS, 5% glycerol and 0.05% bromophenol blue) for 5 min at 37 °C (Kryndushkin *et al.* 2003), and were fractionated by electrophoresis using horizontal 1.8% agarose gels in Tris-Acetate-EDTA (TAE) buffer containing 0.1% SDS.

Western blotting

Proteins were transferred to a polyvinylidene fluoride membrane (Immobilon™, MILLIPORE) and were analyzed by Western blotting. The bound antibody (anti-GFP antibody, a gift from Dr Takayoshi Kuno, anti-Sup35 peptide antibody (Patino *et al.* 1996), and anti-yeast enolase antibody, a gift from Dr Hidetoshi Iida) was detected using by chemiluminescence (ECL, Amersham Biosciences).

Fluorescence correlation spectroscopy

FCS measurements were all performed at 25 °C with a ConfoCor 2 (Carl Zeiss) microscope as described (Saito *et al.* 2003; Weisshart *et al.* 2004). GFP fluorescence was excited at 488 nm with a 6.3 micro W in total power by adjusting the acousto-optical tunable filter (AOTF) to 0.1%. The fluorescence autocorrelation functions (FAF; $G(\tau)$), from which the average residence time (τ_i) and the absolute number of fluorescent proteins in the detection volume are calculated, are obtained as follows;

$$G(\tau) = \frac{[I(t)I(t+\tau)]}{[I(t)]^2} \qquad \text{(eq. 1)}$$

where $I(t + \tau)$ is the fluorescence intensity obtained by the single photon counting method in a detection volume at a delay time τ (brackets denote ensemble averages). The curve fitting for the multicomponent model is given by:

$$G(\tau) = 1 + \frac{1}{N}\sum_i \gamma_i \left(1 + \frac{\tau}{\tau_i}\right)^{-1} \left(1 + \frac{\tau}{s^2\tau_i}\right)^{-1/2} \qquad \text{(eq. 2)}$$

where γ_i and τ_i are the fraction and the diffusion time of the component i, respectively, N is the number of fluorescent molecules in the detection volume defined by the beam waist w_0 and the axial radius z_0, s is the structure parameter representing the ratio of w_0 and z_0. The detection volume made by w_0 and z_0 was approximated to that of a cylinder.

All FAFs in aqueous solutions were measured three times for 30 s at 5 s intervals. In the case of intracellular measurements, FAFs were measured one or three times for 15 s. The effect of photobleaching on FCS analysis was minimized by lowering the excitation intensity and by selecting cells with a low to medium GFP expression level. The measurement position was chosen in the confocal image. Because the optical paths of laser-scanning microscopy (LSM) and FCS are not the same, the real position of the FCS measurement was tuned to the position on the LSM images with a cover glass coated with dried rhodamine 6G (Rh6G), which was the protocol provided by the manufacturer (Weisshart *et al.* 2004). Immediately after each FCS measurement, the cell was again imaged by LSM and checked for displacement. In cases where a cell appeared to have moved, the measurements were discarded. The detection pinhole for FCS was fixed to a diameter of 70 μm and the emission was recorded through a 505–550 nm band pass filter for measurements on living cells. All measured FAFs were fitted by the software installed on the ConfoCor 2 system using the model (eq. 2). FAFs of monomeric GFP in aqueous solution were fitted by a one-component model ($i = 1$). FAFs of monomeric GFP in living cells and of Sup35-GFP in solutions and living cells were fitted by a two-component model ($i = 2$) to estimate a fraction of oligomers. The pinhole adjustment of the FCS setup, the structure parameter, and the detection volume were calibrated for 488 nm excitation each day with a Rh6G solution at a concentration of 10^{-7} M.

Average values of the structure parameter, ranging from 4 to 8, were fixed for FCS analysis throughout this study. The diffusion time of component i, τ_i, is related to the translational diffusion constant D of component i by

$$\tau_i = \frac{w^2}{4D_i} \qquad \text{(eq. 3)}$$

The diffusion of a spherical molecule is related to various physical parameters by the Stokes-Einstein equation as follows.

$$D_i = \frac{\kappa_B T}{6\pi\eta r_i} \qquad \text{(eq. 4)}$$

where T is the absolute temperature, r_i is the hydrodynamic radius of the spherical molecule, η is the fluid-phase viscosity of the solvent, and κ_B is the Boltzman constant. Because τ_i is proportional to viscosity, the relative viscosity ($\tau_{cell}/\tau_{solution}$) can be easily estimated.

Acknowledgements

We thank K. Tanaka and T. Yamamoto for the cultivation of yeast before the FCS measurement, D. Masison, Y. Kimura, B. Ono, R. Tsien, H. Iida and Y. Ohya for the yeast strains and plasmids, S. Kimura for the gift of molecular weight markers and advice about agarose gel electrophoresis, T. Kuno for the gift of anti-GFP antibody, H. Iida for the gift of anti-enolase antibody, and T. Ueda, B.-W. Ying, S. Saito for stimulating discussions. This work was partly supported by a Grant-in aid for Scientific Research no. 16041207 and 17370034 (to H.T.) from the Ministry of Education, Culture, Sports, Science and Technology of Japan, and a Japan Society for the Promotion of Science (JSPS) postdoctoral fellowship for foreign researchers (to C.G.P.).

References

Ayano, S., Noma, S., Yoshida, M., Taguchi, H. & Yasuda, K. (2004) On-chip single-cell observation assay for propagation

dynamics of yeast Sup35 prionlike proteins. *Jpn. J. Appl. Phys.* **43**, 1429–1432.

Bagriantsev, S. & Liebman, S.W. (2004) Specificity of prion assembly in vivo. [PSI+] and [PIN+] form separate structures in yeast. *J. Biol. Chem.* **279**, 51042–51048.

Borchsenius, A.S., Muller, S., Newnam, G.P., Inge-Vechtomov, S.G. & Chernoff, Y.O. (2006) Prion variant maintained only at high levels of the Hsp104 disaggregase. *Curr. Genet.* **49**, 21–29.

Borchsenius, A.S., Wegrzyn, R.D., Newnam, G.P., Inge-Vechtomov, S.G. & Chernoff, Y.O. (2001) Yeast prion protein derivative defective in aggregate shearing and production of new "seeds." *EMBO J.* **20**, 6683–6691.

Bucciantini, M., Giannoni, E., Chiti, F., Baroni, F., Formigli, L., Zurdo, J., Taddei, N., Ramponi, G., Dobson, C.M. & Stefani, M. (2002) Inherent toxicity of aggregates implies a common mechanism for protein misfolding diseases. *Nature* **416**, 507–511.

Campbell, R.E., Tour, O., Palmer, A.E., Steinbach, P.A., Baird, G.S., Zacharias, D.A. & Tsien, R.Y. (2002) A monomeric red fluorescent protein. *Proc. Natl. Acad. Sci. USA* **99**, 7877–7882.

Chien, P., Weissman, J.S. & DePace, A.H. (2004) Emerging principles of conformation-based prion inheritance. *Annu. Rev. Biochem.* **73**, 617–656.

Cleary, J.P., Walsh, D.M., Hofmeister, J.J., Shankar, G.M., Kuskowski, M.A., Selkoe, D.J. & Ashe, K.H. (2005) Natural oligomers of the amyloid-β protein specifically disrupt cognitive function. *Nat. Neurosci.* **8**, 79–84.

Cox, B.S. (1965) [PSI], a cytoplasmic suppressor of supersuppression in yeast. *Heredity* **20**, 505–521.

Cox, B., Ness, F. & Tuite, M. (2003) Analysis of the generation and segregation of propagons: entities that propagate the [PSI+] prion in yeast. *Genetics* **165**, 23–33.

DePace, A.H., Santoso, A., Hillner, P. & Weissman, J.S. (1998) A critical role for amino-terminal glutamine/asparagine repeats in the. *Cell* **93**, 1241–1252.

Derkatch, I.L., Bradley, M.E., Hong, J.Y. & Liebman, S.W. (2001) Prions affect the appearance of other prions: the story of [PIN (+)]. *Cell* **106**, 171–182.

Eaglestone, S.S., Ruddock, L.W., Cox, B.S. & Tuite, M.F. (2000) Guanidine hydrochloride blocks a critical step in the propagation of the prion-like determinant [PSI (+)] of Saccharomyces cerevisiae. *Proc. Natl. Acad. Sci. USA* **97**, 240–244.

Glover, J.R., Kowal, A.S., Schirmer, E.C., Patino, M.M., Liu, J.J. & Lindquist, S. (1997) Self-seeded fibers formed by Sup35, the protein determinant of [PSI+], a heritable prion-like factor of S. cerevisiae. *Cell* **89**, 811–819.

Hess, S.T., Huang, S., Heikal, A.A. & Webb, W.W. (2002) Biological and chemical applications of fluorescence correlation spectroscopy: a review. *Biochemistry* **41**, 697–705.

Inoue, Y., Kishimoto, A., Hirao, J., Yoshida, M. & Taguchi, H. (2001b) Strong growth polarity of yeast prion fiber revealed by single fiber imaging. *J. Biol. Chem.* **276**, 35227–35230.

Inoue, I., Wakamoto, Y., Moriguchi, H., Okano, K. & Yasuda, K. (2001a) On-chip culture system for observation of isolated individual cells. *Laboratory Chip* **1**, 50–55.

Kayed, R., Head, E., Thompson, J.L., McIntire, T.M., Milton, S.C., Cotman, C.W. & Glabe, C.G. (2003) Common structure of soluble amyloid oligomers implies common mechanism of pathogenesis. *Science* **300**, 486–489.

Kim, S., Nollen, E.A., Kitagawa, K., Bindokas, V.P. & Morimoto, R.I. (2002) Polyglutamine protein aggregates are dynamic. *Nat. Cell Biol.* **4**, 826–831.

King, C.Y. (2001) Supporting the structural basis of prion strains: induction and identification of [PSI] variants. *J. Mol. Biol.* **307**, 1247–1260.

King, C.Y., Tittmann, P., Gross, H., Gebert, R., Aebi, M. & Wuthrich, K. (1997) Prion-inducing domain 2–114 of yeast Sup35 protein transforms in vitro into amyloid-like filaments. *Proc. Natl. Acad. Sci. USA* **94**, 6618–6622.

Kishimoto, A., Hasegawa, K., Suzuki, H., Taguchi, H., Namba, K. & Yoshida, M. (2004) β-Helix is a likely core structure of yeast prion Sup35 amyloid fibers. *Biochem. Biophys. Res. Commun.* **315**, 739–745.

Kryndushkin, D.S., Alexandrov, I.M., Ter-Avanesyan, M.D. & Kushnirov, V.V. (2003) Yeast [PSI+] prion aggregates are formed by small Sup35 polymers fragmented by Hsp104. *J. Biol. Chem.* **278**, 49636–49643.

Krzewska, J. & Melki, R. (2006) Molecular chaperones and the assembly of the prion Sup35p, an in vitro study. *EMBO J.* **25**, 822–833.

Lippincott-Schwartz, J., Snapp, E. & Kenworthy, A. (2001) Studying protein dynamics in living cells. *Nat. Rev. Mol. Cell Biol.* **2**, 444–456.

Osherovich, L.Z. & Weissman, J.S. (2001) Multiple Gln/Asn-rich prion domains confer susceptibility to induction of the yeast [PSI(+)] prion. *Cell* **106**, 183–194.

Patino, M.M., Liu, J.J., Glover, J.R. & Lindquist, S. (1996) Support for the prion hypothesis for inheritance of a phenotypic trait in yeast. *Science* **273**, 622–626.

Prusiner, S.B. (1998) Prions. *Proc. Natl. Acad. Sci. USA* **95**, 13363–13383.

Saito, K., Ito, E., Takakuwa, Y., Tamura, M. & Kinjo, M. (2003) In situ observation of mobility and anchoring of PKCbetaI in plasma membrane. *FEBS Lett.* **541**, 126–131.

Salnikova, A.B., Kryndushkin, D.S., Smirnov, V.N., Kushnirov, V.V. & Ter-Avanesyan, M.D. (2005) Nonsense suppression in yeast cells overproducing Sup35 (eRF3) is caused by its non-heritable amyloids. *J. Biol. Chem.* **280**, 8808–8812.

Satpute-Krishnan, P. & Serio, T.R. (2005) Prion protein remodelling confers an immediate phenotypic switch. *Nature* **437**, 262–265.

Serio, T.R., Cashikar, A.G., Moslehi, J.J., Kowal, A.S. & Lindquist, S.L. (1999) Yeast prion [psi+] and its determinant, Sup35p. *Methods Enzymol.* **309**, 649–673.

Sherman, F. (2002) Getting started with yeast. *Methods Enzymol.* **350**, 3–41.

Shkundina, I.S., Kushnirov, V.V., Tuite, M.F. & Ter-Avanesyan, M.D. (2006) The role of the N-Terminal oligopeptide repeats of the yeast Sup35 prion protein in propagation and transmission of prion variants. *Genetics* **172**, 827–835.

Shorter, J. & Lindquist, S. (2005) Prions as adaptive conduits of memory and inheritance. *Nat. Rev. Genet.* **6**, 435–450.

Silveira, J.R., Raymond, G.J., Hughson, A.G., Race, R.E., Sim, V.L., Hayes, S.F. & Caughey, B. (2005) The most infectious prion protein particles. *Nature* **437**, 257–261.

Sondheimer, N. & Lindquist, S. (2000) Rnq1: an epigenetic modifier of protein function in yeast. *Mol. Cell* **5**, 163–172.

Song, Y., Wu, Y.X., Jung, G., Tutar, Y., Eisenberg, E., Greene, L.E. & Masison, D.C. (2005) Role for Hsp70 chaperone in Saccharomyces cerevisiae prion seed replication. *Eukaryot. Cell* **4**, 289–297.

Tuite, M.F. & Cox, B.S. (2003) Propagation of yeast prions. *Nature Rev. Mol. Cell Biol.* **4**, 878–890.

Umehara, S., Wakamoto, Y., Inoue, I. & Yasuda, K. (2003) On-chip single-cell microcultivation assay for monitoring environmental effects on isolated cells. *Biochem. Biophys. Res. Commun.* **305**, 534–540.

Wegrzyn, R.D., Bapat, K., Newnam, G.P., Zink, A.D. & Chernoff, Y.O. (2001) Mechanism of prion loss after Hsp104 inactivation in yeast. *Mol. Cell. Biol.* **21**, 4656–4669.

Weisshart, K., Jungel, V. & Briddon, S.J. (2004) The LSM 510 META—ConfoCor 2 system: an integrated imaging and spectroscopic platform for single-molecule detection. *Curr. Pharm. Biotechnol.* **5**, 135–154.

Weissmann, C. (2004) The state of the prion. *Nat. Rev. Microbiol.* **2**, 861–871.

Wickner, R.B., Edskes, H.K., Ross, E.D., Pierce, M.M., Baxa, U., Brachmann, A. & Shewmaker, F. (2004) Prion genetics: new rules for a new kind of gene. *Annu. Rev. Genet.* **38**, 681–707.

Wu, Y.X., Greene, L.E., Masison, D.C. & Eisenberg, E. (2005) Curing of yeast [PSI+] prion by guanidine inactivation of Hsp104 does not require cell division. *Proc. Natl. Acad. Sci. USA* **36**, 12789–12794.

Zhou, P., Derkatch, I.L. & Liebman, S.W. (2001) The relationship between visible intracellular aggregates that appear after overexpression of Sup35 and the yeast prion-like elements [PSI(+)] and [PIN(+)]. *Mol. Microbiol.* **39**, 37–46.

Received: 17 May 2006
Accepted: 11 June 2006

Supplementary materials

The following supplementary material is available for this article online:

Figure S1 On-chip single cell cultivation system.

Figure S2 Disappearance of the Rnq1-GFP foci in the [*RNQ1*] cell.

Figure S3 FCS measurement of [*GPSI*] cells bearing Sup35-NGMC.

Plant Cell Physiol. 47(8): 1095–1101 (2006)
doi:10.1093/pcp/pcj080, available online at www.pcp.oxfordjournals.org

Fluorescence Cross-Correlation Analyses of the Molecular Interaction between an Aux/IAA Protein, MSG2/IAA19, and Protein–Protein Interaction Domains of Auxin Response Factors of Arabidopsis Expressed in HeLa Cells

Hideki Muto [1], Issei Nagao [2], Taku Demura [3], Hiroo Fukuda [3,4], Masataka Kinjo [2] and Kotaro T. Yamamoto [1,*]

[1] *Division of Biological Sciences, Graduate School of Science, Hokkaido University, Sapporo, 060-0810 Japan*
[2] *Laboratory of Supramolecular Biophysics, Research Institute for Electronic Science, Hokkaido University, Sapporo, 060-0812 Japan*
[3] *Plant Science Center, RIKEN, 1-7-22 Suehiro, Tsurumi-ku, Yokohama, 230-0043 Japan*
[4] *Department of Biological Sciences, Graduate School of Science, The University of Tokyo, Hongo, Tokyo, 113-0033 Japan*

Since auxin may elicit numerous developmental responses by the use of a combination of auxin response factors (ARFs) and their Aux/IAA repressors, it is important to determine the interaction between the two protein families in a quantitative manner. We transiently expressed the C-terminal protein–protein interaction domains (CTDs) of Arabidopsis ARFs, MP/ARF5 and NPH4/ARF7, and MSG2/IAA19, fused to fluorescent proteins in HeLa cells, and determined their molecular interactions with fluorescence cross-correlation spectroscopy (FCCS). Almost complete association was found between MSG2 and MP-CTD and between MSG2 and NPH4-CTD. Approximately 20% association was found for MSG2 homodimers, NPH4-CTD homodimers and MP-CTD/NPH4-CTD heterodimers. Homotypic binding of MP-CTD may be weaker than that of MSG2. MSG2 was localized in cytoplasmic compartments in HeLa cells, whereas it was localized in the nuclei in plant cells. The fact that the heterotypic interaction between MSG2 and ARF-CTDs is stronger than each of the homotypic interactions appears to be the molecular basis for tight control of the transcriptional activity of ARFs by auxin. These results also show that FCCS is useful to examine protein–protein interactions especially for transcriptional regulators.

Keywords: *Arabidopsis thaliana* — Aux/IAA protein — Auxin response factor — Fluorescence cross-correlation spectroscopy — HeLa cell — Protein–protein interaction.

Abbreviations: ARF, auxin response factor; CTD, C-terminal domain; EGFP, enhanced green fluorescent protein; FCCS, fluorescence cross-correlation spectroscopy; FRET, fluorescence resonance energy transfer; mRFP, monomeric red fluorescent protein; tR_2, mRFP tandem dimer.

Introduction

The transcriptional network facilitated by protein–protein interaction appears to play a more important role in the plant kingdom than in other kingdoms, considering that plants have a greater number of plant-specific transcription factors (Riechmann et al. 2000). We have studied the interactions between plant-specific auxin response factors (ARFs) and their repressive regulators, Aux/IAA proteins (IAAs), in a yeast two-hybrid assay (Tatematsu et al. 2004). ARFs and Aux/IAAs share the C-terminal domain (CTD) through which they interact (Kim et al. 1997, Ulmasov et al. 1997). Auxin has been proposed to elicit numerous developmental and physiological responses by the use of a combination of 23 ARFs and 29 Aux/IAAs in a model plant, Arabidopsis (Leyser 2002). Therefore, it is important to determine which Aux/IAAs can associate with each ARF through its CTD in a quantitative manner.

The yeast two-hybrid assay has often been the method of choice to examine interactions between proteins. However, the yeast two-hybrid assay cannot correctly determine the interaction between transcriptional regulators because it uses transcriptional activation as a measure of the protein–protein interaction. Furthermore, the expression levels of tested proteins must be checked separately with other methods such as Western blotting. Thus, new physical methods to detect protein association in vivo have been eagerly awaited. Fluorescence cross-correlation spectroscopy (FCCS) is an emerging technique that can physically evaluate protein–protein interaction in a quantitative manner (Kettling et al. 1998, Rigler et al. 1998). If fluorescence intensity is measured from a small number of fluorophores in a small detection volume, it fluctuates due to the variations in the number of molecules. In such a condition, correlation of fluorescent intensity is calculated over time. For example, two proteins of interest are fused with different fluorescent proteins: one is fused with enhanced green fluorescent protein (EGFP) and the other is fused with monomeric red fluorescent protein (mRFP). Green and red fluorescence signals are measured simultaneously from molecules in a confocal detection volume, and correlation is calculated as a function of time for EGFP and mRFP, respectively, which is called auto-correlation.

*Corresponding author: E-mail, kty@sci.hokudai.ac.jp; Fax, +81-11-706-2739.

Correlation is also calculated between EGFP and mRFP (cross-correlation). If the two fused proteins bind together, a high-amplitude cross-correlation signal will be obtained from fluctuating fluorescence from them. If they move independently, a weak cross-correlation signal will be observed. The population of associated molecules can also be estimated from the calculated auto-correlation function and cross-correlation function.

Fluorescence resonance energy transfer or the Förster resonance energy transfer (FRET) technique is another fluorescent spectroscopic method for studying protein–protein interactions in live cells, in which the efficiency of energy transfer from a donor fluorophore bound to one protein to an acceptor fluorophore on the other protein is determined. It has been used more often than FCCS (Miyawaki 2003), and is completely different from FCCS which is based on thermal fluctuation of molecules. A disadvantage of FRET is that FRET efficiency greatly depends on the distance and angle between the donor and acceptor fluorophores. The efficiency is poor if the distance between the two fluorophores is greater than a few nanometers. Furthermore, the emission spectrum of the donor fluorophor should overlap with the excitation spectrum of the acceptor fluorophore. In contrast, any combinations of two spectrally distinct fluorescent probes are utilized for FCCS analysis irrespective of their relative geometry because FCCS is based on only the coincidence of the two fluorescences. In principle, therefore, FCCS is free from the limitations of FRET (Takagi et al. 2004). The two methods also differ from each other with respect to data acquisition: most in vivo FRET experiments are based on the ratio image of fluorescence intensity from sequentially acquired images collected by a laser scanning microscope or a charge-coupled device (CCD) camera. On the other hand, standard FCCS equipment does not provide simultaneous measurements at many points in cells, and thus does not provide an image for visualizing the subcellular localization of fluorophores.

Here, we have used FCCS to investigate the interaction between MSG2/IAA19 (Tatematsu et al. 2004) and MP/ARF5- or NPH4/ARF7-CTDs (Hardtke and Berleth 1998, Harper et al. 2000, Hamann et al. 2002), which were transiently expressed as fusion proteins with the fluorescent proteins in HeLa cells. Through this study, we also show that the FCCS method can be successfully applied to the analysis and measurement of plant protein interactions, broadening its use from the few in vitro and in vivo model systems reported so far (Bacia et al. 2002, Kim et al. 2004, Saito et al. 2004, Baudendistel et al. 2005).

Results and Discussion

We first estimated maximum cross-correlation by measuring the cross-correlation of EGFP fused to the mRFP tandem dimer (tR_2) expressed in HeLa cells (Figs. 1, 2b). EGFP and tR_2 separately expressed in one cell were also examined for minimum cross-correlation (Fig. 2a). Determination with these cell lines resulted in a $74.8 \pm 10.7\%$ cross ratio $[(G_c(0)-1)/(G_r(0)-1)]$ for the maximum cross-correlation and a $23.3 \pm 5.5\%$ cross ratio for the minimum cross-correlation (Fig. 3). When MSG2 fused to EGFP was expressed with MP-CTD fused to tR_2, a $73.0 \pm 13.9\%$ cross ratio was observed (Fig. 2c). Essentially the same interaction was obtained for a reverse combination of fusion proteins, EGFP–MP-CTD and tR_2–MSG2 (Fig. 3). These values coincided with the maximum value of the cross ratio, indicating complete association between MSG2 and MP-CTD. Essentially the same results were obtained for the interaction between MSG2 and NPH4-CTD (Fig. 2d). On the other hand, the cross ratio between EGFP–MSG2 and tR_2–MSG2 was $33.7 \pm 6.2\%$ (Fig. 2e), which was significantly higher than the minimum value of the cross ratio ($P = 0.0054$ by Student's t-test). It was also higher than that for interaction between two fluorescent proteins, only one of which was fused with MSG2 (one-sided free fluorescent protein

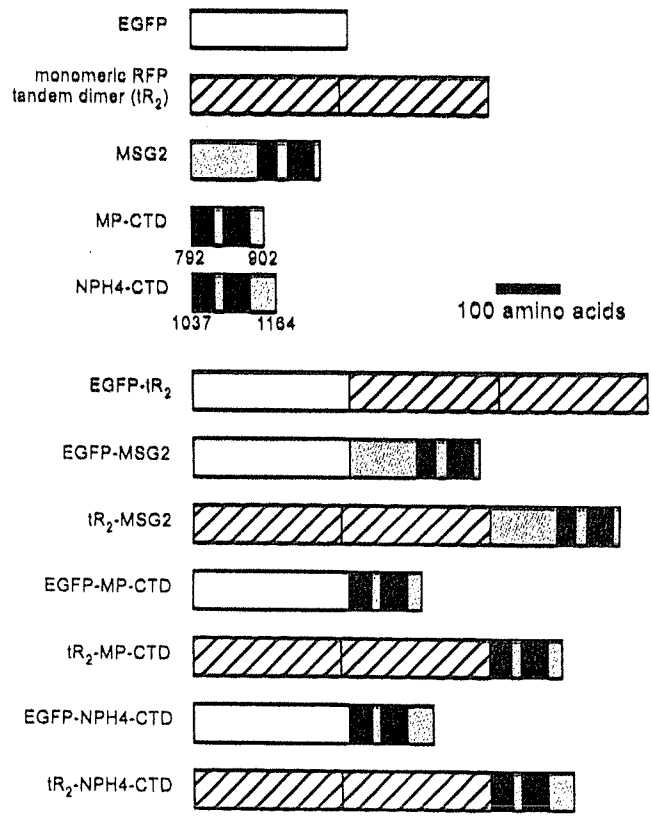

Fig. 1 Schematic drawing of fusion proteins expressed in this study. Black boxes represent domains III and IV of the C-terminal domain (CTD) which is conserved in ARFs and Aux/IAAs. Numbers below the CTDs indicate amino acid numbers of the N- and C-termini of CTDs.

controls: $P<0.026$). If we assume that the maximum and minimum cross ratios correspond to 100 and 0% association, respectively, about 20% of MSG2 molecules are judged to form a homodimer. Values for the homotypic interaction of MP- and NPH4-CTD and those for the heterotypic interaction between MP-CTD and NPH4-CTD (Fig. 2f) were all similar in magnitude to that between MSG2 monomers, which were significantly larger than the minimum cross ratio ($P<0.017$ for all combinations). The homotypic interaction between NPH4-CTD and the heterotypic interaction between MP- and NPH4-CTD were also significantly higher than that of the one-sided free fluorescent protein controls ($P<0.022$), except for the interaction between EGFP–MP-CTD and free tR_2 ($P>0.20$). On the other hand, the homodimeric interaction between MP-CTD molecules was as weak as that of the one-sided free fluorescent protein controls ($P>0.137$), suggesting that homotypic interaction of MP-CTD was negligible.

When MSG2–GFP was transiently expressed in onion epidermal cells by the use of particle bombardment, it was exclusively found in the nucleus (Fig. 4a). However, EGFP–MSG2 was seen diffusively in the cytoplasm as well as in the nucleus when expressed in HeLa cells (Fig. 4c). Although tR_2–MSG2 was also present in both compartments, it was excluded from the nucleus more readily than EGFP–MSG2 (Fig. 4d), probably due to its larger molecular size (72.5 kDa) than EGFP–MSG2 (48.4 kDa). EGFP–MSG2 was found almost exclusively in the cytoplasm when co-expressed with tR_2–NPH4-CTD (65.4 kDa; Fig. 4h), which was found in both the cytoplasm and nucleus when expressed alone (Fig. 4g). These results

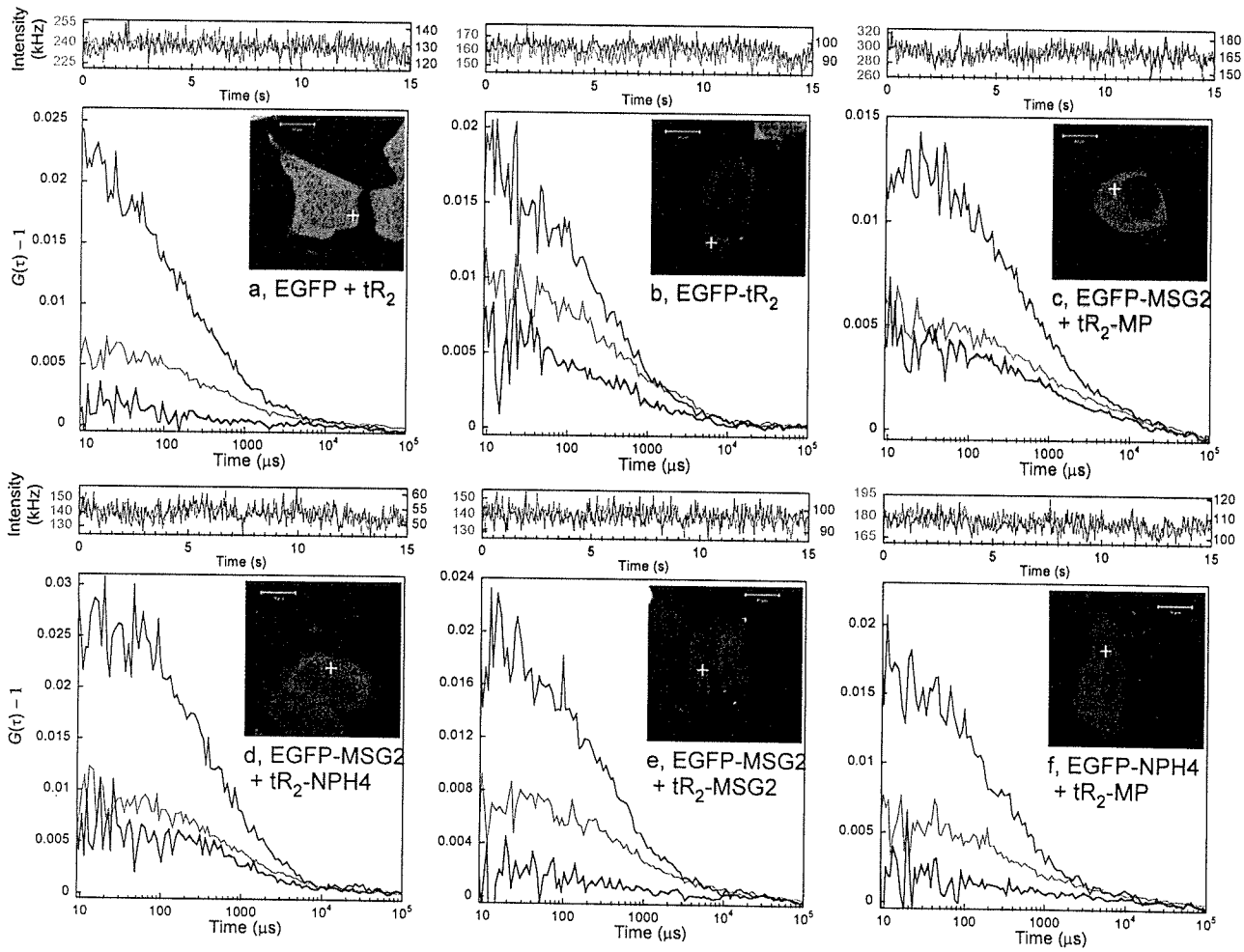

Fig. 2 Cross-correlation analyses. Typical auto- and cross-correlation curves of EGFP and tR_2 (a), EGFP–tR_2 (b), EGFP–MSG2 and tR_2–MP-CTD (c), EGFP–MSG2 and tR_2–NPH4-CTD (d), EGFP–MSG2 and tR_2–MSG2 (e), and EGFP–NPH4-CTD and tR_2–MP-CTD (f) expressed in HeLa cells. The fluorescence intensities in the red and green channels are shown in the upper graph of each panel in red and blue, respectively. Auto-correlation curves for red and green channels, and a cross-correlation curve between the two colors are depicted in the lower graph of each panel in red, blue and black, respectively. Intensity of fluorescence was measured at cross hairs in each inset with a 10-μm scale bar.

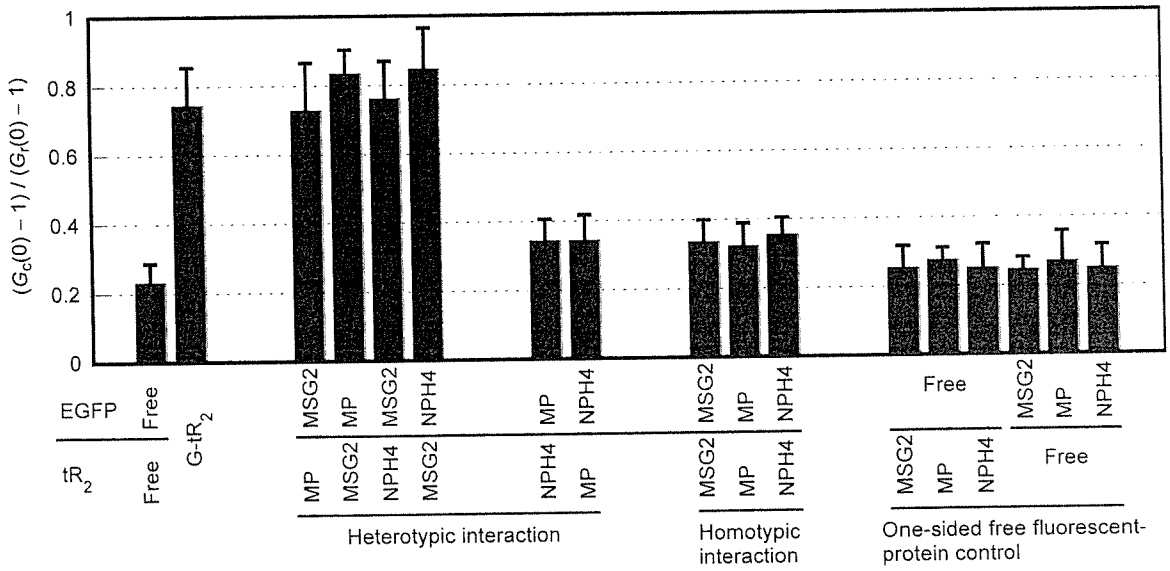

Fig. 3 Cross ratio $[(G_c(0)—1)/(G_r(0)—1)]$ determined with FCCS, which corresponds to the fraction of the associated molecules (N_c/N_g). MSG2 and MP- and NPH4-CTDs were fused with EGFP or tR_2. Values shown are the mean and SD of 4–9 measurements.

strongly suggest that EGFP–MSG2 interacted with tR_2–NPH4-CTD so strongly that the resultant complexes were efficiently excluded from the nucleus because of their large molecular size. The subcellular localization of EGFP–MSG2 was not affected by the presence of either tR_2–MSG2 (Fig. 4i) or tR2 (Fig. 4j), suggesting that there was no significant interaction between the MSG2 monomer molecules. Essentially the same results were obtained between EGFP–MSG2 and tR_2–MP-CTD (data not shown).

In this study, we were able to determine the protein–protein interaction between MSG2 and MP- or NPH4-CTDs in a quantitative manner with FCCS. Almost complete association was observed between MSG2 and ARF-CTDs, while ~20% association was found between MSG2 monomers. Homodimeric interaction between NPH4-CTD monomers and heterodimeric interaction between MP- and NPH4-CTDs are also similar in strength to homodimeric interaction between MSG2 molecules. The interaction between MP-CTD monomers may be more subtle (Fig. 3). These results imply that Aux/IAA and ARF proteins primarily exist as a heterodimeric form between the two protein families. When one of them cannot find its partner, it is often present in a monomeric form; homodimeric species and heterodimeric species between ARFs are found on fewer occasions. This conclusion is consistent with the observed subcellular localization of EGFP–MSG2 in HeLa cells, which is affected by the expression of tR_2–NPH4-CTD, but not by tR_2–MSG2 (Fig. 4). The strong interaction between Aux/IAA and ARF suggests that transcriptional regulation conducted by ARFs is readily modified by the change in Aux/IAA level, which is under the direct control of the auxin F-box receptors (Dharmasiri et al. 2005, Kepinski and Leyser 2005).

The molecular interaction between Aux/IAA proteins and ARF-CTDs has been investigated with the yeast two-hybrid system (Kim et al. 1997, Ulmasov et al. 1997, Ouellet et al. 2001, Hamann et al. 2002, Hardtke et al. 2004, Tatematsu et al. 2004, Fukaki et al. 2005, Weijers et al. 2005, Weijers et al. 2006) and immunoprecipitation (Tatematsu et al. 2004, Weijers et al. 2006). Homotypic interaction of IAA1, AXR3/IAA17 or its CTD was observed with size exclusion chromatography (Kim et al. 1997) or electrophoretic (Ouellet et al. 2001) and cross-linking methods (Kim et al. 1997). Stronger interaction between MSG2 and MP- or NPH4-CTD than each homodimeric interaction was reported by the use of the yeast two-hybrid assay (Tatematsu et al. 2004). Similar results were obtained between BDL/IAA12 and MP- or NPH4-CTD (Hardtke et al. 2004, Weijers et al. 2005, Weijers et al. 2006) and between AXR3 and ARF1 (Ouellet et al. 2001). When maximum interaction was evaluated as the activity of the reporter gene in the presence of the GAL4 transcription factor in the yeast two-hybrid system, the interactions between MSG2 and MP- or NPH4-CTD were ~30% of the maximum interaction in our previous study (Tatematsu et al. 2004). A slightly stronger interaction was detected between BDL and MP- or NPH4-CTD (Hardtke et al. 2004). Furthermore, only 0.9% of the

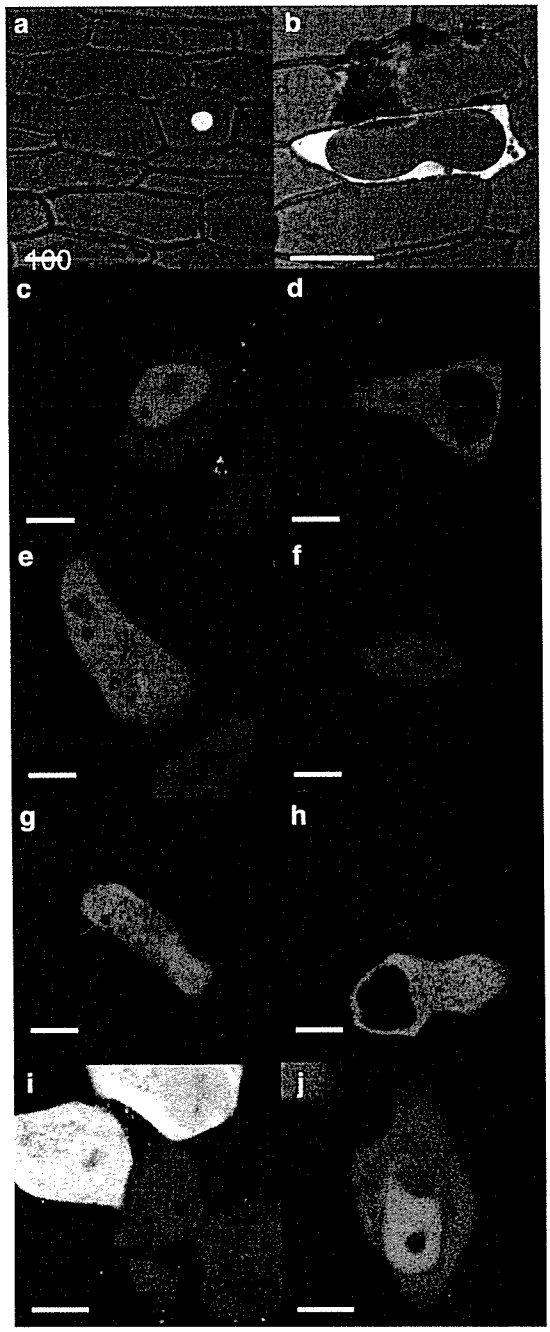

Fig. 4 Subcellular localization of MSG2 and NPH4-CTD fused with EGFP, tR_2 or GFP. Proteins were transiently expressed in the onion epidermal cells (a and b) or HeLa cells (c–j). (a) MSG2–GFP. (b) Free GFP. (c) EGFP–MSG2. (d) tR_2–MSG2. (e) Free EGFP. (f) Free tR_2. (g) tR_2–NPH4-CTD. (h) EGFP–MSG2 and tR_2–NPH4-CTD. (i) EGFP–MSG2 and tR_2–MSG2. (j) EGFP–MSG2 and free tR_2. Scale bars, 100 μm in a and b, and 10 μm in c–j.

maximum interaction was observed between MSG2 monomers (Tatematsu et al. 2004). On the other hand, BDL formed a homodimer as readily as it produced a heterodimer with MP-CTD (Hamann et al. 2002). Although these results cannot be directly compared with those of the present FCCS experiments, they appear to be in sharp contrast to almost complete association between MSG2 and ARF-CTDs and ~20% association between MSG2 in the FCCS study. The difference probably arises from the repressive nature of Aux/IAA proteins in transcription, which has been well characterized in plant cells (Tiwari et al. 2004). This clearly illustrates the limitation of the yeast system and the marked advantage of the physical FCCS method to evaluate protein–protein interaction between transcription factors quantitatively. On the other hand, the interaction between MSG2 monomers appears to be near the limit of detection for FCCS, although it would be detected easily by the yeast two-hybrid assay if it is not a transcriptional repressor. This seems to represent a weakness of FCCS. Recently, the interaction between GFP-fused BDL and HA (hemagglutinin epitope)-tagged MP was examined in planta with immunoprecipitation. When protein extracts were immunoprecipitated with anti-HA antibody, almost all the BDL was recovered in precipitates, indicating that BDL primarily exists as a heterodimer with MP in flower buds (Weijers et al. 2006). This is consistent with our observation that MSG2 binds to ARFs more strongly than it binds to itself.

Two oncoproteins, Fos and Jun, are transcription factors of the basic region leucine zipper (bZIP) type. Since they act as a heterodimer, the thermodynamics of their dimerization has been intensively studied. A dissociation constant of ~50 nM was reported for their peptides that consisted of the basic DNA-binding region and leucine zipper motif (Kohler and Schepartz 2001). Baudendistel et al. (2005) also investigated the interaction between the whole Fos and Jun proteins in HeLa cells with FCCS. If we assume that the maximum and minimum cross ratios correspond to 100 and 0% association, respectively, again, ~60% of the oncoproteins are estimated to form a heterodimer in HeLa cells. The maximum cross-correlation observed in the present study (~80%) is much higher than that (45%) reported by Baudendistel et al. (2005). This seems to be due to a few improvements in our experiments: narrowing the confocal detection volume for the green channel, and brightening fluorescence in the red channel by the use of tR_2 instead of mRFP in their work. Expressing plant proteins in human cells may also be important because plant proteins artificially expressed in HeLa cells may interact with each other freely without interference by endogenous ARFs, Aux/IAAs or other interacting plant proteins. However, this could also be a drawback of our FCCS analyses since the protein interaction was observed in a non-native environment. In this connection, it is interesting to note that the subcellular localization of MSG2 in HeLa cells (Fig. 4)

is totally different from the consistent nuclear localization of Aux/IAAs in plant cells reported previously (Fig. 4a; Abel et al. 1994, Abel and Theologis 1995, Ouellet et al. 2001, Fukaki et al. 2002, Hamann et al. 2002, Weijers et al. 2006). Aux/IAA proteins contain conserved nuclear localization signals (Abel et al. 1994, Abel and Theologis 1995, Ouellet et al. 2001). The results suggest that HeLa cells may lack efficient molecular machineries to recognize the nuclear localization signal of plant-specific Aux/IAAs or to transport them into the nucleus.

In conclusion, we have shown that FCCS is a useful physical technique to determine molecular interaction quantitatively, which complements the use of conventional biological or immunochemical approaches. Using FCCS, we show that MSG2 mostly exists as a heterodimer with NPH4- or MP-CTD in HeLa cell cytoplasm. The strong association between MSG2 and ARFs may make it possible for auxin to control the transcriptional activity of ARFs tightly through changes in the MSG2 level.

Materials and Methods

The nucleotide sequence for MSG2, MP- or NPH4-CTD was amplified by PCR from cDNA using a pair of oligonucleotide primers: 5′-GTCGACATGGAGAAGGAAGGACTCGG-3′ and 5′-GCATGCGGACCCGGGCTCGTCTACTCCTCT-3′ for MSG2; 5′-GTCGACGTCCGAACCTACACTAAGGTT-3′ and 5′-CCCGGGTGAAACAGAAGTCTTAAGATC-3′ for MP-CTD; and 5′-GTCGACATGCGAACTTATACAAAGGTG-3′ and 5′-CCCGGGCCGGTTAAACGAAGTGGCTGA-3′ for NPH4-CTD. All the forward and reverse primers contained *Sal*I and *Sma*I sites respectively, at their 5′ ends. The PCR product was subcloned into pT7-blue (Novagen, San Diego, CA, USA) digested with *Eco*RV, and its sequence was confirmed by sequencing. After digestion with *Sal*I and *Sma*I, the inserted DNA was cloned downstream of EGFP in pEGFP-C1 (Clontech, Mountain View, CA, USA) or tR_2 in the tR_2-replaced pEGFP-C1 (Saito et al. 2004).

For expression in onion (*Allium cepa*) epidermal cells, the nucleotide sequence for MSG2 was amplified as described above with the exception of the forward primer, 5′-CACCATGGAGAAGGAAGGACTCGG-3′. The PCR product was subcloned into pENTR-D-TOPO (Invitrogen, Carlsbad, CA, USA). The GFP gene was amplified by PCR using forward and reverse primers containing *Sma*I and *Sph*I sites, respectively, at their 5′ ends. The PCR product was inserted between the *Sma*I and *Sph*I sites at the 3′ end of the MSG2 sequence. The DNA fragment, *MSG2::GFP*, was inserted downstream of the cauliflower mosaic virus 35S promoter of the gateway binary vector pH35GS (Kubo et al. 2005), using LR clonase (Invitrogen). pBI121-GFP was used for free GFP (Sugikawa et al. 2005). These plasmids were introduced into onion epidermal cells by particle bombardment (PDS-1000/He, Bio-Rad, Hercules, CA, USA) using 1.0 μm gold particles at 1,100 p.s.i. After incubation in MS medium (Murashige and Skoog 1962) for 24 h, the onion cells were examined with a confocal laser scanning microscope (LSM410; Zeiss, Oberkochen, Germany).

HeLa cells were grown as described elsewhere (Saito et al. 2004). Transfection was carried out on LAB-TEK chambered coverslips with eight wells (Nalge Nunc, Rochester, NY, USA), using FuGENE 6 (Roche, Basel, Switzerland). During FCCS measurements, HeLa cells were maintained in Opti-MEM I reduced serum medium (Invitrogen). FCCS measurements were carried out with a ConfoCor2 (Zeiss) (Saito et al. 2004), which consisted of a CW Ar^+ laser and a He–Ne laser, a water immersion objective (C-Apochromat, 40×, 1.2NA; Zeiss) and two channels of avalanche photodiodes (SPCM-200-PQ; EG&G, Gaithersberg, MD, USA). EGFP and tR_2 were excited at 488 and 543 nm, respectively. The confocal pinhole diameter was adjusted to 40 and 78 μm for the 488 and 543 nm laser lines, respectively. The emission signals were split by a dichroic mirror (570 nm beam splitter) and detected at 505–530 nm by the green channel for EGFP and at >610 nm by the red channel for tR_2.

Fluorescence data were processed in essentially the same manner as described by Saito et al. (2004). In brief, the fluorescence auto-correlation functions of the red and green channels, $G_r(\tau)$ and $G_g(\tau)$, are calculated by

$$G_x(\tau) = \langle I_x(t) I_x(t+\tau) \rangle / (\langle I_x(t) \rangle \langle I_x(t) \rangle),$$

where τ represents the time delay, I_x is the fluorescence intensity in the green ($x = g$) or red channel ($x = r$), and $\langle\rangle$ denotes the time average (for 15 s in this study). The cross-correlation function, $G_c(\tau)$, is given by

$$G_c(\tau) = \langle I_g(t) I_r(t+\tau) \rangle / (\langle I_g(t) \rangle \langle I_r(t) \rangle).$$

The average number of fluorescent molecules, N, in the confocal detection volume was calculated by resolving the observed $G(\tau)$ into a two-component model. Then, the average numbers of red fluorescent molecules (N_r), green fluorescent molecules (N_g) and molecules that emit both red and green lights (N_c) were calculated by

$$N_r = 1/(G_r(0) - 1),\ N_g = 1/(G_g(0) - 1),$$
$$N_c = (G_c(0) - 1)/[(G_r(0) - 1)(G_g(0) - 1)].$$

We usually carried out FCCS measurements in the condition that $N_g < N_r$ but that their molar ratio was near one. Therefore, the ratio of the associated molecules to the sum of the associated and the monomeric molecules corresponded to N_c/N_g, which was given by the cross ratio, $[G_c(0)-1]/[G_r(0)-1]$.

Fluorescence images of live cells were obtained with an inverted confocal laser scanning microscope LSM510 (Zeiss) (Saito et al. 2004), using the same laser lines described above. Emission signals were detected at 505–550 nm for EGFP and at >560 nm for tR_2 by sequential scanning.

Acknowledgments

We are grateful to Drs. Y. Niwa (University of Shizuoka) and K. Yamazaki (Hokkaido University) for pBI121-GFP. This work was supported in part by Grants-in-Aid for Scientific Research from the Japan Society for the Promotion of Science to H.M. (17770026) and M.K. (15370062), and from the Ministry of Education, Culture, Sports, Science, and Technology to M.K. (17050001) and K.T.Y. (14036201).

References

Abel, S., Oeller, P.W. and Theologis, A. (1994) Early auxin-induced genes encode short-lived nuclear proteins. *Proc. Natl. Acad. Sci. USA* 91: 326–330.

Abel, S. and Theologis, A. (1995) A polymorphic bipartite motif signals nuclear targeting of early auxin-inducible proteins related to PS-IAA4 from pea (*Pisum sativum*). *Plant J.* 8: 87–96.

Bacia, K., Majoul, I.V. and Schwille, P. (2002) Probing the endocytic pathway in live cells using dual-color fluorescence cross-correlation analysis. *Biophys. J.* 83: 1184–1193.

Baudendistel, N., Müller, G., Waldeck, W., Angel, P. and Langowski, J. (2005) Two-hybrid fluorescence cross-correlation spectroscopy detects protein–protein interactions in vivo. *Chem. Phys. Chem.* 6: 984–990.

Dharmasiri, N., Dharmasiri, S. and Estelle, M. (2005) The F-box protein TIR1 is an auxin receptor. *Nature* 435: 441–445.

Fukaki, H., Nakao, Y., Okushima, Y., Theologis, A. and Tasaka, M. (2005) Tissue-specific expression of stabilized SOLITARY-ROOT/IAA14 alters lateral root development in Arabidopsis. *Plant J.* 44: 382–395.

Fukaki, H., Tameda, S., Masuda, H. and Tasaka, M. (2002) Lateral root formation is blocked by a gain-of-function mutation in the *SOLITARY-ROOT/IAA14* gene of *Arabidopsis*. *Plant J.* 29: 153–168.

Hamann, T., Benkova, E., Bäurle, I., Kientz, M. and Jürgens, G. (2002) The *Arabidopsis BODENLOS* gene encodes an auxin response protein inhibiting MONOPTEROS-mediated embryo patterning. *Genes Dev.* 16: 1610–1615.

Hardtke, C.S. and Berleth, T. (1998) The *Arabidopsis* gene *MONOPTEROS* encodes a transcription factor mediating embryo axis formation and vascular development. *EMBO J.* 17: 1405–1411.

Hardtke, C.S., Ckurshumova, W., Vidaurre, D.P., Singh, S.A., Stamatiou, G., Tiwari, S.B., Hagen, G., Guilfoyle, T.J. and Berleth, T. (2004) Overlapping and non-redundant functions of the *Arabidopsis* auxin response factors *MONOPTEROS* and *NONPHOTOTROPIC HYPOCOTYL 4*. *Development* 131: 1089–1100.

Harper, R.M., Stowe-Evans, E.L., Luesse, D.R., Muto, H., Tatematsu, K., Watahiki, M.K., Yamamoto, K. and Liscum, E. (2000) The *NPH4* locus encodes the auxin response factor ARF7, a conditional regulator of differential growth in aerial Arabidopsis tissue. *Plant Cell* 12: 757–770.

Kepinski, S. and Leyser, O. (2005) The Arabidopsis TIR1 protein is an auxin receptor. *Nature* 435: 446–451.

Kettling, U., Koltermann, A., Schwille, P. and Eigen, M. (1998) Real-time enzyme kinetics monitored by dual-color fluorescence cross-correlation spectroscopy. *Proc. Natl. Acad. Sci. USA* 95: 1416–1420.

Kim, J., Harter, K. and Theologis, A. (1997) Protein–protein interactions among the Aux/IAA proteins. *Proc. Natl. Acad. Sci. USA* 94: 11786–11791.

Kim, S.A., Heinze, K.G., Waxham, M.N. and Schwille, P. (2004) Intracellular calmodulin availability accessed with two-photon cross-correlation. *Proc. Natl. Acad. Sci. USA* 101: 105–110.

Kohler, J. and Schepartz, A. (2001) Kinetic studies of Fos·Jun·DNA complex formation: DNA binding prior to dimerization. *Biochemistry* 40: 130–142.

Kubo, M., Udagawa, M., Nishikubo, N., Horiguchi, G., Yamaguchi, M., Ito, J., Mimura, T., Fukuda, H. and Demura, T. (2005) Transcription switches for protoxylem and metaxylem vessel formation. *Genes Dev.* 19: 1855–1860.

Leyser, O. (2002) Molecular genetics of auxin signaling. *Annu. Rev. Plant Biol.* 53: 377–398.

Miyawaki, A. (2003) Visualization of the spatial and temporal dynamics of intracellular signaling. *Dev. Cell* 4: 295–305.

Murashige, T. and Skoog, F. (1962) A revised medium for rapid growth and bio assays with tobacco tissue cultures. *Physiol. Plant.* 15: 473–497.

Ouellet, F., Overvoorde, P.J. and Theologis, A. (2001) IAA17/AXR3: biochemical insight into an auxin mutant phenotype. *Plant Cell* 13: 829–841.

Riechmann, J.L., Heard, J., Martin, G., Reuber, L., Jiang, C.-Z., *et al.* (2000) *Arabidopsis* transcription factors: genome-wide comparative analysis among eukaryotes. *Science* 290: 2105–2110.

Rigler, R., Földes-Papp, Z., Meyer-Almes, F.-J., Sammet, C., Völcker, M. and Schnetz, A. (1998) Fluorescence cross-correlation: a new concept for polymerase chain reaction. *J. Biotechnol.* 63: 97–109.

Saito, K., Wada, I., Tamura, M. and Kinjo, M. (2004) Direct detection of caspase-3 activation in single live cells by cross-correlation analysis. *Biochem. Biophys. Res. Commun.* 324: 849–854.

Sugikawa, Y., Ebihara, S., Tsuda, K., Niwa, Y. and Yamazaki, K. (2005) Transcriptional coactivator MBF1s from *Arabidopsis* predominantly localize in nucleolus. *J. Plant Res.* 118: 431–437.

Takagi, T., Kii, H. and Kinjo, M. (2004) DNA measurements by using fluorescence correlation spectroscopy and two-color fluorescence cross-correlation spectroscopy. *Curr. Pharm. Biotechnol.* 5: 199–204.

Tatematsu, K., Kumagai, S., Muto, H., Sato, A., Watahiki, M.K., Harper, R.M., Liscum, E. and Yamamoto, K.T. (2004) *MASSUGU2* encodes Aux/IAA19, an auxin-regulated protein that functions together with the transcriptional activator NPH4/ARF7 to regulate differential growth responses of hypocotyl and formation of lateral roots in Arabidopsis. *Plant Cell* 16: 379–393.

Tiwari, S.B., Hagen, G. and Guilfoyle, T.J. (2004) Aux/IAA proteins contain a potent transcriptional repression domain. *Plant Cell* 16: 533–543.

Ulmasov, T., Hagen, G. and Guilfoyle, T.J. (1997) ARF1, a transcription factor that binds to auxin response elements. *Science* 276: 1865–1868.

Weijers, D., Benkova, E., Jäger, K.E., Schlereth, A., Hamann, T., Kientz, M., Wilmoth, J.C., Reed, W.R. and Jürgens, G. (2005) Developmental specificity of auxin response by pairs of ARF and Aux/IAA transcription regulators. *EMBO J.* 24: 1874–1885.

Weijers, D., Schlereth, A., Ehrismann, J.S., Schwank, G., Kientz, M. and Jürgens, G. (2006) Auxin triggers transient local signaling for cell specification in *Arabidopsis* embryogenesis. *Dev. Cell* 10: 265–270.

(Received April 1, 2006; Accepted June 20, 2006)

nature
biotechnology

A fluorescent variant of a protein from the stony coral *Montipora* facilitates dual-color single-laser fluorescence cross-correlation spectroscopy

Takako Kogure[1], Satoshi Karasawa[1–3], Toshio Araki[1–3], Kenta Saito[4], Masataka Kinjo[4] & Atsushi Miyawaki[1]

Dual-color fluorescence cross-correlation spectroscopy (FCCS) is a promising technique for quantifying protein-protein interactions[1–5]. In this technique, two different fluorescent labels are excited and detected simultaneously within a common measurement volume. Difficulties in aligning two laser lines and emission crossover between the two fluorophores, however, make this technique complex. To overcome these limitations, we developed a fluorescent protein with a large Stokes shift. This protein, named Keima, absorbs and emits light maximally at 440 nm and 620 nm, respectively. Combining a monomeric version of Keima with cyan fluorescent protein allowed dual-color FCCS with a single 458-nm laser line and complete separation of the fluorescent protein emissions. This FCCS approach enabled sensitive detection of proteolysis by caspase-3 and the association of calmodulin with calmodulin-dependent enzymes. In addition, Keima and a spectral variant that emits maximally at 570 nm might facilitate simultaneous multicolor imaging with single-wavelength excitation.

Dual-color FCCS has several advantages over standard fluorescence correlation spectroscopy (FCS). Whereas FCS detects molecular concentrations and mobility[3], FCCS enables the tracing of two spectrally distinguishable fluorophores, thus extracting essential information about the kinetics of molecular interactions[1–5]. FCCS requires two fluorophores of different colors. For simultaneous excitation of the two fluorophores, two lasers are aligned to the same confocal spot. Bringing two laser beams to a perfect and stable overlap, however, is often difficult. Although FCCS can be performed using a single laser line (SL-FCCS) for single-photon excitation[6], complex mathematical computations are required to compensate for cross-excitation, cross-talk and fluorescence resonance energy transfer (FRET) when common fluorophores that have broad excitation and emission spectra and modest Stokes shifts are used. Thus, simple SL-FCCS has been achieved only with special fluorophores, such as 'MegaStokes' dyes (http://www.dyomics.com/), although some innovative techniques for specific labeling of recombinant proteins with organic dyes[7] might render the MegaStokes dyes more applicable. One solution for efficient simultaneous excitation may come from two-photon excitation (TPE) microscopy[8]; two differently colored fluorophores can be excited simultaneously by a single infrared, ultra-short pulse laser line because of the blue-shift effect. Although TPE-SL-FCCS performs well[9–12], it requires expensive equipment and specialized expertise. Also, in TPE, the rate of bleaching per unit excitation increases supralinearly with pulse intensity[13,14]. This increase may add another decay component, thereby complicating analyses.

The development of fluorescent proteins with large Stokes shifts has long been pursued to create a fluorescent protein pair in which the two fluorescent proteins have comparable excitation maxima but sufficiently different Stokes shifts. To identify such candidate proteins, we used degenerate primers[15] to amplify cDNAs constructed from the stony coral *Montipora* sp. One clone was selected that encoded a new green fluorescent protein (GFP)-like protein. The protein, referred to as no. 20, is a violet-colored chromoprotein that does not fluoresce. Its absorption spectrum at pH 7.4 shows a major absorption maximum at 576 nm ($\varepsilon = 64{,}000\ M^{-1}\ cm^{-1}$) with a slight shoulder at ~535 nm (**Fig. 1a**). Sequence analysis revealed that no. 20 is closely related to a chromoprotein from *Goniopora tenuidens* gtCP[16]. An amino-acid alignment of no. 20 with DsRed is shown in **Supplementary Fig. 1** online.

To efficiently evolve the chromoprotein into a useful fluorescent protein, we carried out semi-random mutagenesis[17]. Random substitutions of several amino acids whose side chains were close to the chromophore were simultaneously introduced into the protein. Five substitutions (H94N, N142S, N157D, K202R and F206S) and the addition of a valine residue at the second amino-acid position resulted in a red fluorescent protein (no. 20-9115). This protein showed an emission spectrum peaking at 606 nm and a bimodal excitation spectrum peaking at 452 and 580 nm (**Fig. 1b**). A pH titration experiment revealed that the two excitation peaks corresponded to the neutral and ionized states of the phenolic hydroxyl moiety of the chromophore, respectively[18] (data not shown). To simplify the excitation spectrum, we used semi-random mutagenesis to shift the neutralization/ionization equilibrium to either of the two states. A new

[1]Laboratory for Cell Function and Dynamics, Advanced Technology Development Group, Brain Science Institute, RIKEN, 2-1 Hirosawa, Wako-city, Saitama, 351-0198, Japan. [2]Amalgaam Co., Ltd. 2-9-3 Itabashi, Itabashi-ku, Tokyo, 173-0004, Japan. [3]Medical & Biological Laboratories Co., Ltd., 3-5-10 Marunouchi, Naka-ku, Nagoya-city, 460-0002, Japan. [4]Research Institute for Electronic Science, Hokkaido University, Sapporo, 060-0812, Japan. Correspondence should be addressed to A.M. (matsushi@brain.riken.jp).

Received 18 November 2005; accepted 29 March 2006; published online 30 April 2006; doi:10.1038/nbt1207

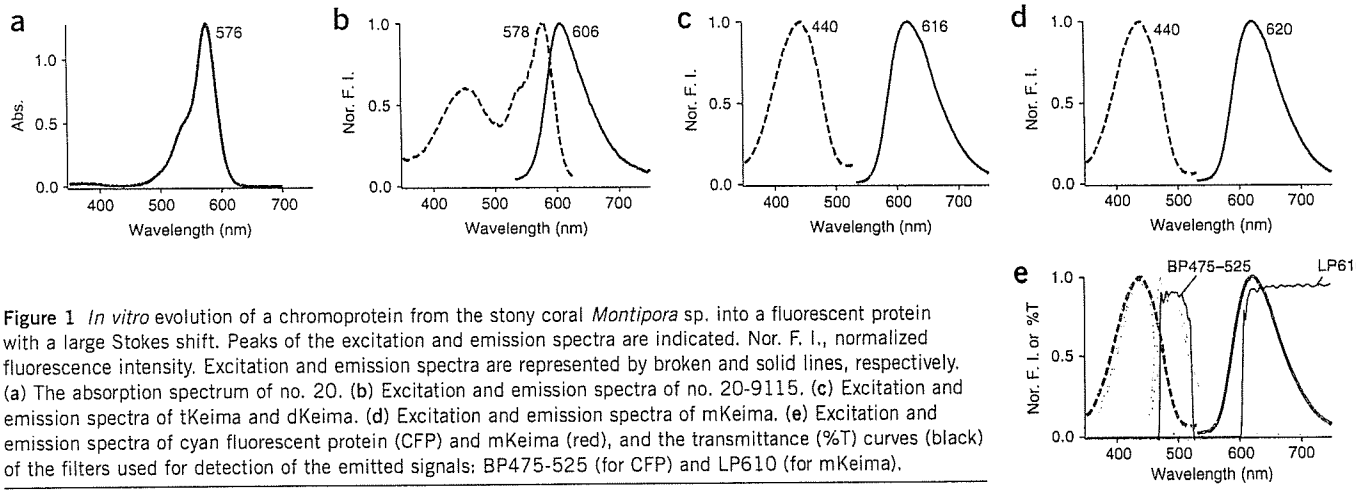

Figure 1 *In vitro* evolution of a chromoprotein from the stony coral *Montipora* sp. into a fluorescent protein with a large Stokes shift. Peaks of the excitation and emission spectra are indicated. Nor. F. I., normalized fluorescence intensity. Excitation and emission spectra are represented by broken and solid lines, respectively. (**a**) The absorption spectrum of no. 20. (**b**) Excitation and emission spectra of no. 20-9115. (**c**) Excitation and emission spectra of tKeima and dKeima. (**d**) Excitation and emission spectra of mKeima. (**e**) Excitation and emission spectra of cyan fluorescent protein (CFP) and mKeima (red), and the transmittance (%T) curves (black) of the filters used for detection of the emitted signals: BP475-525 (for CFP) and LP610 (for mKeima).

fluorescent protein with four mutations (S61F, I92T, F158Y and S213A) seemed to exist principally in the neutral state; the 580-nm peak was substantially reduced. Additionally, compared with those of no. 20-9115, the excitation peak of the neutral state and the emission peak were slightly blue-shifted and red-shifted, respectively. As a result, the protein absorbs light maximally at 440 nm and emits a far-red fluorescence maximally at 616 nm (**Fig. 1c**). Owing to the large Stokes shift, we named the protein 'Keima,' a shogi (Japanese chess) piece that hops in the manner of the knight in chess.

The absolute molecular mass of Keima was determined to be 106 kDa by analytical equilibrium ultracentrifugation analysis (**Supplementary Fig. 2a** online). This value was four times larger than the 25-kDa value deduced from the primary structure of the protein, suggesting that Keima forms a homotetrameric complex (referred to hereafter as 'tKeima'). At pH 7.4, the molar extinction coefficient (ε) at 440 nm and fluorescence quantum yield (Φ) of tKeima were 14,500 M^{-1} cm^{-1} and 0.22, respectively. The monomeric version of DsRed was previously generated by altering 33 amino-acid residues[19]. Assuming that the structure of tKeima is similar to that of the DsRed tetramer, we introduced V123T into the AB interface. Another mutation (V191I) was introduced to increase the folding efficiency of the mutant. The absolute molecular mass of 52.2 kDa (**Supplementary Fig. 2b**) was almost twice the predicted size of the monomer. This dimeric protein was named 'dKeima.' Compared to tKeima, dKeima showed the same absorption spectrum peaking at 440 nm (ε = 24,600 M^{-1} cm^{-1}), the same excitation/emission spectra (**Fig. 1c**) and a Φ of 0.31. After numerous cycles of semi-random mutagenesis, we successfully inhibited the formation of the AC dimer by introducing seven additional mutations (L60Q, F61L, V79F, T92S, T123E, Y188R and Y190E) to produce 'mKeima,' a monomeric protein. The absolute molecular mass of mKeima was 31 kDa (**Supplementary Fig. 2c**). mKeima showed the same spectra as tKeima and dKeima except that the emission maximum was 620 nm (**Fig. 1d**). The ε at 440 nm and Φ of mKeima were 14,400 M^{-1} cm^{-1} and 0.24, respectively. The mutations introduced into no. 20 to form mKeima are summarized in **Supplementary Fig. 1**. Additionally, the spectral characteristics of tKeima, dKeima and mKeima are summarized in **Supplementary Table 1** online.

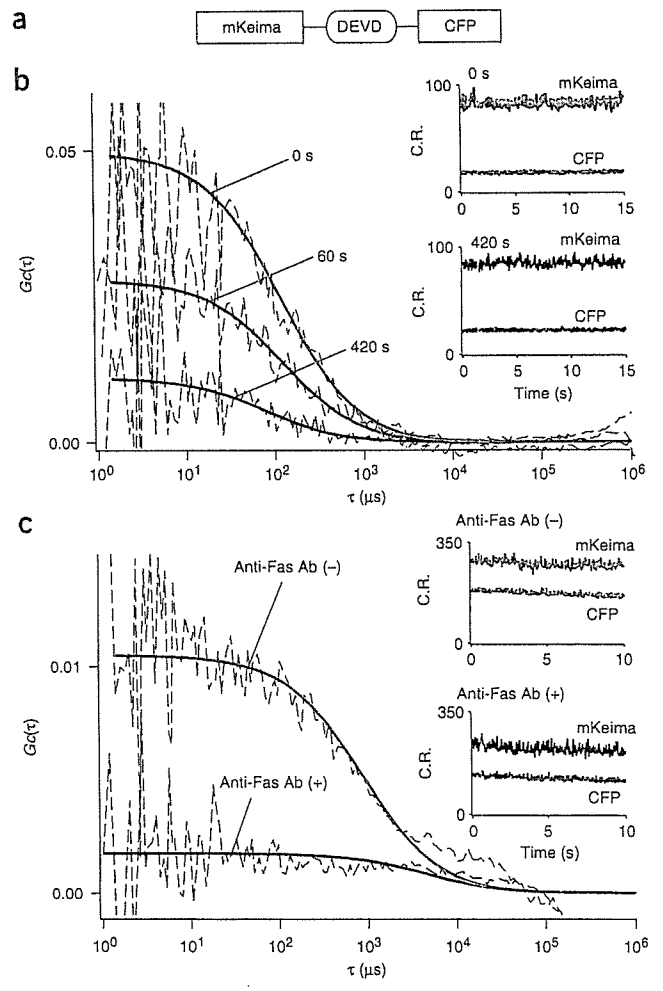

Figure 2 Single laser wavelength (458 nm) excitation FCCS using mKeima and CFP to monitor proteolysis by caspase-3. (**a**) A schematic representation of the primary structure of the caspase-3 sensor protein. (**b**) *In vitro* cross-correlation analysis. Cross-correlation curves measured at 0 s (red), 60 s (black) and 420 s (blue) after the addition of caspase-3. (**c**) Cross-correlation analysis in live HeLa cells. Cross-correlation curves measured from anti-Fas antibody-treated (blue) and untreated (red) cells expressing the sensor protein. (**b**,**c**) $Gc(\tau)$, the cross-correlation function. Insets: the fluorescence intensities of mKeima and CFP in the two respective channels during an FCCS measurement. C.R., count rates.

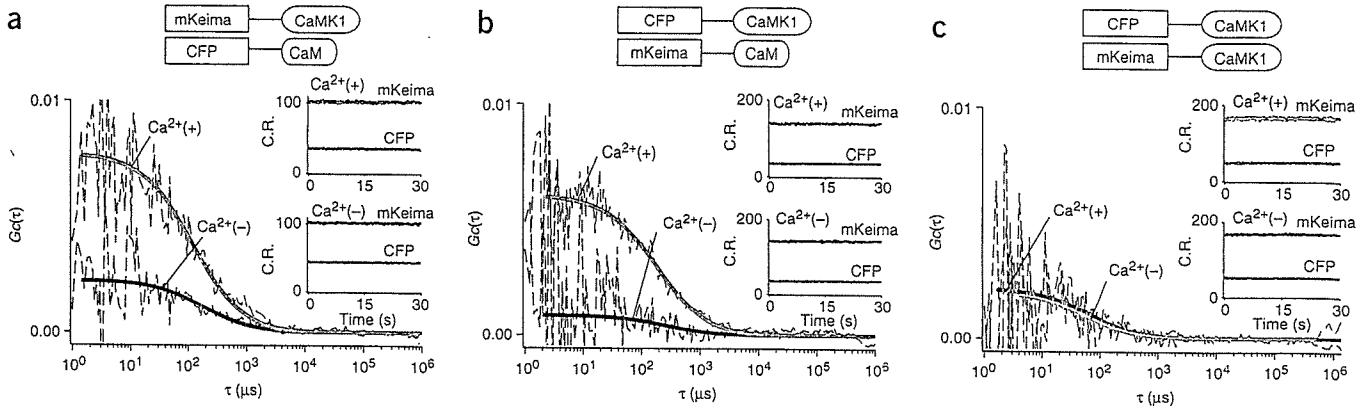

Figure 3 Single laser wavelength (458 nm) excitation FCCS using mKeima and CFP to monitor the Ca^{2+}-dependent association between CaM and CaMKI. Cross-correlation curves were measured in the presence of 0.1 mM EGTA (blue, $Ca^{2+}(-)$) and then after the addition of 1 mM $CaCl_2$ (red, $Ca^{2+}(+)$). $Gc(\tau)$: the cross-correlation function. Insets: the fluorescence intensities of mKeima and CFP in the two respective channels during an FCCS measurement. C.R., count rates. (**a**) mKeima-CaMKI and CFP-CaM. (**b**) CFP-CaMKI and mKeima-CaM. (**c**) CFP-CaMKI and mKeima-CaMKI.

We tried to establish an SL-FCCS system solely based on fluorescent proteins. Combined use of a cyan-emitting variant of *Aequorea victoria* GFP (CFP)[18] and mKeima permitted simple but efficient SL-FCCS, because the two fluorescent proteins possess nearly identical excitation spectra and completely separable emission spectra (**Fig. 1e**). Also, there is no FRET between CFP and Keima.

The C terminus of mKeima and the N terminus of CFP (ECFP) were linked using a peptide containing the caspase-3 cleavage sequence DEVD (**Fig. 2a**). The recombinant protein (mKeima-DEVD-CFP) was examined in a chamber using an excitation wavelength of 458 nm. Substantial cross-correlation was observed between the fluctuations in the two detection channels (**Fig. 2b**, 0 s). Incubation of the same sample with activated recombinant caspase-3 (0.2 U/μl) at 25 °C for 7 min almost completely abolished the cross-correlation signal (**Fig. 2b**, 420 s). The linear relationship between the relative cross-correlation and the percentage of intact substrate was verified in a separate experiment in which several mixtures containing various ratios of intact caspase-3 substrates (mKeima-DEVD-CFP) to purified mKeima and CFP were used to measure cross-correlation signals (**Supplementary Fig. 3a** online). The proteolysis was then examined in apoptotic cells. The same FCCS experiments were conducted with HeLa cells transfected with cDNA coding for mKeima-DEVD-CFP. The degree of cross-correlation was substantially different between anti-Fas antibody-treated and untreated cells (**Fig. 2c**). It is important to note that in an mKeima-DEVD-CFP-expressing HeLa cell, mKeima and CFP were photobleached with similar kinetics during strong irradiation at 440 nm (**Supplementary Fig. 3b**).

Next we applied the FCCS technique to the detection of the Ca^{2+}-dependent association between calmodulin (CaM) and CaM-dependent kinase I (CaMKI). mKeima and CFP were fused to the N termini of CaMKI and CaM, respectively, to generate mKeima-CaMKI and CFP-CaM (**Fig. 3a**). The two fusion proteins were prepared separately using a wheat germ *in vitro* translation system. FCCS was then performed using a mixture of the two samples. The amplitude of the cross-correlation was low in the absence of Ca^{2+} (0.1 mM EGTA) (**Fig. 3a**, $Ca^{2+}(-)$), but increased after the addition of 1 mM $CaCl_2$ (**Fig. 3a**, $Ca^{2+}(+)$). A similar result was obtained with a combination of two alternative fusion proteins, CFP-CaMKI and mKeima-CaM (**Fig. 3b**). On the other hand, the cross-correlation for a mixture of CFP-CaMKI and mKeima-CaMKI was negligible irrespective of the level of Ca^{2+} (**Fig. 3c**). In addition, mKeima or CFP was fused to the C terminus of CaMKI or CaM to make CaMKI-mKeima, CaMKI-CFP, CaM-mKeima and CaM-CFP. Using these eight constructs, we tried all eight of the potential CaM/CaMKI combinations in FCCS experiments to monitor the association between CaM and CaMKI. A Ca^{2+}-dependent increase in cross-correlation was detected in seven of the eight combinations (see **Supplementary Fig. 4** online). No increase was observed for the mixture of CaM-mKeima and

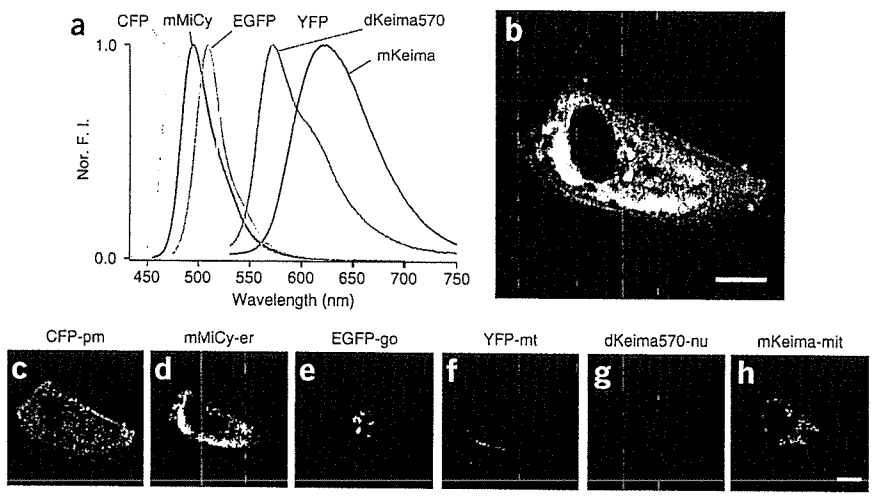

Figure 4 Simultaneous six-color imaging of subcellular structures in a Vero cell using a single laser line (458 nm). (**a**) Normalized emission spectra of CFP, mMiCy, EGFP, YFP, dKeima570 and mKeima. (**b**) An image of the Vero cell with CFP localized on the plasma membrane (yellow), mMiCy in the endoplasmic reticulum (cyan), EGFP in the Golgi (green), YFP along the microtubules (red), dKeima570 in the nucleus (dark blue) and mKeima in the mitochondria (purple). The image was created by merging the following images, which were obtained using spectral imaging: CFP-pm (**c**), mMiCy-er (**d**), EGFP-go (**e**), YFP-mt (**f**), dKeima570-nu (**g**) and mKeima-mit (**h**). Scale bars, 10 μm.

CaMKI-CFP, possibly because of disruption of the CaM/CaMKI interaction by one of the fusions. As detection of molecular associations by FCCS is usually not affected by fusion design or the size of the host proteins, this technique is applicable to high-throughput screening of interacting protein pairs. By contrast, FRET efficiency is highly sensitive to the way in which the two fluorescent proteins are fused to the host proteins; substantial effort will be required to obtain fusion constructs that give significant changes in the FRET signal upon CaM/CaMKI association.

Reversible molecular interactions should be harder to detect in live cells than in *in vitro* experiments; because cells contain endogenous unlabeled molecules, which can interfere with the association between two distinct, fluorescently labeled species, FCCS signals might be attenuated. Introducing more labeled molecules into live cells might overwhelm this interference. Unlike FRET, however, FCCS requires that the concentrations of labeled molecules are kept low to optimize the fluctuating signals. We used cell samples that had been transfected with the cDNAs for CaM-CFP and M13 (the CaM-binding peptide of myosin light chain kinase)[20]-mKeima. Despite an excess amount of endogenous, unlabeled CaM and CaM-binding proteins, a Ca^{2+}-dependent increase in the cross-correlation signal was detected (see **Supplementary Fig. 5** online), evidence for the applicability of FCCS in transfection-based experiments, which to our knowledge has not been experimentally supported before. It should be noted that the interference problem does not apply to the detection of proteolysis by FCCS, because the cross-correlation signals from double-labeled substrates should not be affected by endogenous substrates.

To test the applicability of mKeima for multicolor imaging, we simultaneously imaged the cytosolic free Ca^{2+} concentration ($[Ca^{2+}]_c$) and mitochondrial morphology in highly motile cell samples. We cotransfected rat cardiac muscle cells with cDNAs that encoded a variant of yellow cameleon (YC3.60)[21], a Ca^{2+} indicator containing CFP and yellow fluorescent protein (YFP)[18], and a mitochondrially targeted variant of mKeima (mKeima-mit). Images of CFP, YFP and mKeima fluorescence were simultaneously acquired using a color camera (AQUACOSMOS/ASHURA, Hamamatsu Photonics) operating in the stream mode at video rate. Also, to improve the spatial resolution along the *z*-axis, a spinning disk unit (CSU21, Yokogawa) was placed in front of the camera. We observed contracting movement of the cell and mitochondria with contraction-coupled increases in the $[Ca^{2+}]_c$, which was monitored using YC3.60 (see **Supplementary Fig. 6** online).

During the semi-random mutagenesis of dKeima, whose emission spectrum peaks at 616 nm, we found that two additional substitutions (F61M and Q62C) shifted the emission peak to 570 nm without affecting the excitation spectrum or dimer formation (see **Supplementary Figs. 1, 2d, 7** and **Supplementary Table 1** online). This dimeric variant was named dKeima570. We then labeled living cells with a large set of spectrally different dyes that could be excited with a single laser line. We tried to label subcellular structures in living cells with six different fluorescent proteins that can be excited at 458 nm: CFP, mMiCy[22] (H. Suzuki, S.K. and A.M., unpublished data), EGFP[18], YFP, dKeima570 and mKeima (**Fig. 4**). The emission spectra of these proteins overlap to various degrees (**Fig. 4a**). With the appropriate targeting signals, the fluorescent proteins were localized to the plasma membrane (CFP-pm), endoplasmic reticulum (mMiCy-er), Golgi apparatus (EGFP-go), microtubules (YFP-mt), nucleus (dKeima570-nu) or mitochondria (mKeima-mit). Vero cells expressing all six of the proteins were visualized using a 458-nm argon laser line 2 d after cotransfection. Using a commercially available confocal microscopy system, the six emission signals were precisely and efficiently separated (**Fig. 4c–h**). An image of the superimposed signals (**Fig. 4b**) helps to clarify the dynamic interactions of subcellular structures in living cells. Thus, Keima and its variants solve longstanding problems in multicolor imaging technology, such as accurate laser alignment and excitation chromatic effects, although problems caused by emission chromatic effects have yet to be resolved.

METHODS

cDNA cloning and gene construction. A sample of the stony coral *Montipora* sp. was acquired from the ocean near the Okinawa islands by K. Iwao (Akajima Marine Science Laboratory). Total RNA was isolated from the corals by guanidine thiocyanate extraction. Synthesis, amplification using degenerate primers and generation of full-length cDNAs were carried out as previously described[23]. The degenerate primers 5′-GAAGGRTGYGTCAAYGGRCAY-3′ and 5′-ACVGGDCCATYDGVAAGAAARTT-3′ covered several regions that coded for amino-acid sequences that are conserved among GFP-like fluorescent proteins from a number of Anthozoa species[15]. The missing 5′ and 3′ ends of a cDNA fragment were amplified using the RACE strategy. cDNA encoding the protein-coding region was amplified using primers containing 5′ *Bam*HI and 3′ *Eco*RI sites. For bacterial expression, the digested product was then cloned in-frame into the *Bam*HI/*Eco*RI sites of $pRSET_B$ (Invitrogen). To promote efficient translation, the 5′ end of the gene was modified by PCR to contain a Kozak consensus sequence (CCACCATG) after the *Bam*HI site. The *Bam*HI/*Eco*RI fragment was then subcloned into the mammalian expression vector pcDNA3 (Invitrogen).

Mutagenesis. Site-directed and semi-random mutations were introduced as described[17,24]. Pairs of amino-acid residues that surrounded the chromophore and had side chains oriented toward the chromophore were mutated. A degenerative primer was designed for each strand so that the two residues would be randomly replaced with other amino acids. Also, multiple primer sets were used to simultaneously introduce random mutations at selected sites. *Escherichia coli* cells transformed with mutagenized plasmids were screened on agar plates for red fluorescence using the fluorescence image analyzing system described previously[24].

Protein expression, *in vitro* spectroscopy and pH titrations. Fluorescent proteins were expressed in *E. coli*, purified and characterized spectroscopically as previously described[23]. Fluorescence quantum yields were determined using fluorescein as a standard (0.91). For the calculation of molar extinction coefficients, protein concentrations were measured using a Bradford assay kit (Bio-Rad) and bovine serum albumin as the standard. pH titrations were performed as described[23].

Analytical ultracentrifugation. Sedimentation equilibrium experiments were performed using a Beckman XL-1 analytical ultracentrifuge at 20 °C. Absorbance was measured at the maximum wavelength as a function of radius at rotor speeds of $18.1 \times 10^3 g$ and $50.3 \times 10^3 g$ and protein concentrations of 0.125, 0.25 and 0.5 absorbance units. Using this analytical system, the tetramerization of DsRed was verified.

FCCS. The LSM 510 META/ConfoCor 2 system (Carl Zeiss) equipped with an Ar ion laser was used. The excitation line was set at 458 nm. The excitation beam was reflected by a HFT458 dichroic mirror and focused by a water immersion objective lens (C-Apochromat 40X/NA1.2; Carl Zeiss). The emitted light was collimated and then split by a NFT570 dichroic mirror. Emission signals were detected through a BP475-525 emission filter for CFP and a LP610 emission filter for mKeima. The transmittance curves of the two emission filters are shown in **Fig. 1e**. Data analysis was done as described[4]. The acquired $G(\tau)$ function was fitted by a one-component model as

$$G(\tau) = \frac{1}{N}\left(1+\frac{\tau}{\tau_1}\right)^{-1}\left(1+\frac{\tau}{s^2\tau_1}\right)^{-1/2}$$

where τ_1 is the diffusion time of the fluorescent particles, N is the average number of fluorescent particles in the excitation-detection volume defined by the radius w_0 and length $2z_0$, and s is the structure parameter representing the

ratio $s = z_0/w_0$. For quantitative evaluation, $Gc(0)$ (the amplitude of the cross-correlation function) is divided by $Gk(0)$ (the amplitude of the autocorrelation function of mKeima) to calculate the relative cross-correlation ($Gc(0)/Gk(0)$).

Monitoring the association between CaM and CaMKI. Recombinant proteins containing CaM/CaMKI and mKeima/CFP were generated using PROTEIOS, a wheat germ cell-free protein synthesis core kit (TOYOBO). The products were concentrated using VIVASPIN (VIVASCIENCE). Mixtures of two samples were analyzed by FCCS. The association between CaM and CaMKI was blocked by adding 0.1 mM EGTA and then achieved by adding 1 mM $CaCl_2$.

Proteolysis analysis. mKeima-DEVD-CFP was expressed in *E. coli* and purified as previously described[23]. The protein (10 nM) was incubated at 25 °C with activated caspase-3 (MBL) (0.2 U/μl) in buffer containing 20 mM HEPES-KOH (pH 7.5), 10 mM KCl, 1.5 mM $MgCl_2$, 1 mM EDTA, 1 mM EGTA and 1 mM dithiothreitol. Two days after transfection with the cDNA coding for mKeima-DEVD-CFP, HeLa cells in HBSS (Invitrogen) were treated with 100 ng/ml anti-Fas antibodies (CH-11; MBL) and cyclohexamide (10 μg/ml)[25].

Multicolor imaging. EGFP-go, YFP-mt, dKeima570-nu and mKeima-mit were constructed by fusing the 81 N-terminal amino acids of the type II membrane-anchored protein galactosyltransferase[26], the human wild-type tau four-repeat[27], the nuclear localization signal from poly(ADP-ribose) polymerase (S.K., T.A. and A.M., unpublished results) and the 29 N-terminal amino acids of the cytochrome *c* oxidase subunit VIII presequence[28] to the N termini of EGFP (Clontech), YFP, dKeima570 and mKeima, respectively. CFP-pm was generated by fusing the 20 C-terminal amino acids of K-Ras[29] to the C terminus of ECFP (Clontech). mMiCy-er was generated by extending mMiCy at the N terminus with the signal peptide from calreticulin and at the C terminus with an ER retention signal[30]. cDNAs coding for the chimeric proteins were transfected into Vero cells using Lipofectamine 2000 (Invitrogen). Spectra imaging with a single laser line at 458 nm (Ar ion laser) was performed using the 32 channels of the LSM 510 META system (Carl Zeiss).

Accession codes. DNA Data Bank of Japan: the sequences reported in this paper have been deposited with accession nos. AB209967, AB209968 and AB209969.

Note: Supplementary information is available on the Nature Biotechnology website.

ACKNOWLEDGMENTS

The authors would like to thank K. Iwao and S. Hosaka at the Akajima Marine Science Laboratory for acquiring the stony coral animals, Y. Isogai for assistance with analytical centrifugation, F. Ishidate, K. Weisshart, B. Zimmerman, Y. Hasegawa for assistance with FCCS measurements and spectral imaging, and K. Ishihara, H. Watanabe, T. Fukano, and M. Hirano for assistance with multi-color imaging and fluorescence lifetime measurements. This work was partly supported by grants from Japan MEXT Grant-in-Aid for Scientific Research on priority areas, NEDO (the New Energy and Industrial Technology Development Organization), HFSP (the Human Frontier Science Program), and RIKEN Strategic Research Program.

COMPETING INTERESTS STATEMENT

The authors declare competing financial interests (see the *Nature Biotechnology* website for details).

Published online at http://www.nature.com/naturebiotechnology/
Reprints and permissions information is available online at http://npg.nature.com/reprintsandpermissions/

1. Kettling, U., Koltermann, A., Schwille, P. & Eigen, M. Real-time enzyme kinetics monitored by dual-color fluorescence cross-correlation spectroscopy. *Proc. Natl. Acad. Sci. USA* **95**, 1416–1420 (1998).
2. Weidemann, T., Wachsmuth, M., Tewes, M., Rippe, K. & Langowski, J. Analysis of ligand binding by two-colour fluorescence cross-correlation spectroscopy. *Single Mol.* **3**, 49–61 (2002).
3. Kim, S.A. & Schwille, P. Intracellular applications of fluorescence correlation spectroscopy: prospects for neuroscience. *Curr. Opin. Neurobiol.* **13**, 583–590 (2003).
4. Saito, K., Wada, I., Tamura, M. & Kinjo, M. Direct detection of caspase-3 activation in single live cells by cross-correlation analysis. *Biochem. Biophys. Res. Commun.* **324**, 849–854 (2004).
5. Kohl, T., Haustein, E. & Schwille, P. Determining protease activity in vivo by fluorescence cross-correlation analysis. *Biophys. J.* **89**, 2770–2782 (2005).
6. Hwang, L.C. & Wohland, T. Single wavelength excitation fluorescence cross-correlation spectroscopy with spectrally similar fluorophores: Resolution for binding studies. *J. Chem. Phys.* **122**, 114708 (1–11) (2005).
7. Martin, B.R., Giepmans, B.N., Adams, S.R. & Tsien, R.Y. Mammalian cell-based optimization of the biarsenical-binding tetracysteine motif for improved fluorescence and affinity. *Nat. Biotechnol.* **23**, 1308–1314 (2005).
8. Helmchen, F. & Denk, W. New developments in multiphoton microscopy. *Curr. Opin. Neurobiol.* **12**, 593–601 (2002).
9. Heinze, K.G., Koltermann, A. & Schwille, P. Simultaneous two-photon excitation of distinct labels for dual-color fluorescence crosscorrelation analysis. *Proc. Natl. Acad. Sci. USA* **97**, 10377–10382 (2000).
10. Kohl, T., Heinze, K.G., Kuhlemann, R., Koltermann, A. & Schwille, P. A protease assay for two-photon crosscorrelation and FRET analysis based solely on fluorescent proteins. *Proc. Natl. Acad. Sci. USA* **99**, 12161–12166 (2002).
11. Heinze, K.G., Rarbach, M., Jahnz, M. & Schwille, P. Two-photon fluorescence coincidence analysis: rapid measurements of enzyme kinetics. *Biophys. J.* **83**, 1671–1681 (2002).
12. Kim, S.A., Heinze, K.G., Waxham, M.N. & Schwille, P. Intracellular calmodulin availability accessed with two-photon cross-correlation. *Proc. Natl. Acad. Sci. USA* **101**, 105–110 (2004).
13. Patterson, G.H. & Piston, D.W. Photobleaching in two-photon excitation microscopy. *Biophys. J.* **78**, 2159–2162 (2000).
14. Chen, T.S., Zeng, S.Q., Luo, Q.M., Zhang, Z.H. & Zhou, W. High-order photobleaching of green fluorescent protein inside live cells in two-photon excitation microscopy. *Biophys. Biochem. Res. Commun.* **291**, 1272–1275 (2002).
15. Matz, M.V., Lukyanov, K.A. & Lukyanov, S.A. Family of the green fluorescent protein: journey to the end of the rainbow. *Bioessays* **24**, 953–959 (2002).
16. Labas, Y.A. *et al.* Diversity and evolution of the green fluorescent protein family. *Proc. Natl. Acad. Sci. USA* **99**, 4256–4261 (2002).
17. Tsutsui, H., Karasawa, S., Shimizu, H., Nukina, N. & Miyawaki, A. Semi-rational engineering of a coral fluorescent protein into an efficient highlighter. *EMBO Rep.* **6**, 233–238 (2005).
18. Tsien, R.Y. The green fluorescent protein. *Annu. Rev. Biochem.* **67**, 509–544 (1998).
19. Campbell, R.E. *et al.* A monomeric red fluorescent protein. *Proc. Natl. Acad. Sci. USA* **99**, 7877–7882 (2002).
20. Crivici, A. & Ikura, M. Molecular and structural basis of target recognition by calmodulin. *Annu. Rev. Biophys. Biomol. Struct.* **24**, 85–116 (1995).
21. Nagai, T., Yamada, S., Tominaga, T., Ichikawa, M. & Miyawaki, A. Expanded dynamic range of fluorescent indicators for Ca^{2+} by circularly permuted yellow fluorescent proteins. *Proc. Natl. Acad. Sci. USA* **101**, 10554–10559 (2004).
22. Karasawa, S., Araki, T., Nagai, T., Mizuno, H. & Miyawaki, A. Cyan-emitting and orange-emitting fluorescent proteins as a donor/acceptor pair for fluorescence resonance energy transfer. *Biochem. J.* **381**, 307–312 (2004).
23. Karasawa, S., Araki, T., Yamamoto-Hino, M. & Miyawaki, A. A green-emitting fluorescent protein from Galaxeidae coral and its monomeric version for use in fluorescent labeling. *J. Biol. Chem.* **278**, 34167–34171 (2003).
24. Sawano, A. & Miyawaki, A. Directed evolution of green fluorescent protein by a new versatile PCR strategy for site-directed and semi-random mutagenesis. *Nucleic Acids Res.* **28**, E78 (2000).
25. Arscott, P.L. *et al.* Fas (CD95) expression is up-regulated on papillary thyroid carcinoma. *J. Clin. Endocrinol. Metab.* **84**, 4246–4252 (1999).
26. Llopis, J., McCaffery, J.M., Miyawaki, A., Farquhar, M.G. & Tsien, R.Y. Measurement of cytosolic, mitochondrial, and Golgi pH in single living cells with green fluorescent proteins. *Proc. Natl. Acad. Sci. USA* **95**, 6803–6808 (1998).
27. Sato, S. *et al.* Aberrant tau phosphorylation by glycogen synthase kinase-3b and JNK3 induces oligomeric tau fibrils in COS-7 cells. *J. Biol. Chem.* **277**, 2060–2065 (2002).
28. Sawano, A., Hama, H., Saito, N. & Miyawaki, A. Multicolor imaging of Ca^{2+} and protein kinase C signals using novel epifluorescence microscopy. *Biophys. J.* **82**, 1076–1085 (2002).
29. Mochizuki, N. *et al.* Spatio-temporal images of growth-factor-induced activation of Ras and Rap1. *Nature* **411**, 1065–1068 (2001).
30. Miyawaki, A. *et al.* Fluorescent indicator for Ca^{2+} based on green fluorescent proteins and calmodulin. *Nature* **388**, 882–887 (1997).

Available online at www.sciencedirect.com
SCIENCE DIRECT
ELSEVIER
Analytical Biochemistry 350 (2006) 196–201
ANALYTICAL BIOCHEMISTRY
www.elsevier.com/locate/yabio

Detection of oxidative stress-induced mitochondrial DNA damage using fluorescence correlation spectroscopy

Yasutomo Nomura [a,*], Hirobumi Fuchigami [b], Hiroaki Kii [c], Zhonggang Feng [b], Takao Nakamura [a], Masataka Kinjo [c]

[a] *Department of Environmental Life Science, Graduate School of Medical Science, Yamagata University, Yonezawa, Yamagata 992-8510, Japan*
[b] *Department of Bio-System Engineering, Faculty of Engineering, Yamagata University, Yonezawa, Yamagata 992-8510, Japan*
[c] *Laboratory of Supramolecular Biophysics, Research Institute for Electronic Science, Hokkaido University, Sapporo 060-0812, Japan*

Received 5 September 2005
Available online 25 January 2006

Abstract

Using fluorescence correlation spectroscopy (FCS), we tested the feasibility of rapid detection of oxidative damage of mitochondrial DNA (mtDNA) in a small volume. The complete mtDNA genome was amplified by long polymerase chain reaction (LPCR), and the product was fluorescently labeled with an intercalating dye, YOYO-1. The fluorescence autocorrelation function was analyzed using a simple two-component model with the diffusion time of 0.21 ms for the LPCR primer and 18 ms for the mtDNA LPCR product. When human embryonic kidney 293 (HEK-293) cells were exposed to 0.4 mM H_2O_2, the fraction of the mtDNA LPCR product decreased significantly. In contrast, the fraction of the nuclear-encoded β-globin LPCR product remained unchanged. The analysis time of FCS measurement was very short (5 min) compared with that of gel electrophoresis (3 h). Thus, FCS allowed the rapid detection of the vulnerability of mtDNA to oxidative stress within a small volume element at the subfemtoliter level in solution. These results suggest that the LPCR–FCS method can be used for epidemiological studies of diseases caused by mtDNA damage.

Keywords: Fluorescence correlation spectroscopy; Long PCR; Mitochondria; Oxidative stress

Damaged mitochondrial DNA (mtDNA)[1] has been reported to be involved in a variety of human diseases, including diabetes, cancer, Parkinson's disease, and Alzheimer's disease [1,2]. However, the factors responsible for the damage in the diseases remain to be determined. Major candidates for the primary source of damage may be reactive oxygen species (ROS). Mitochondria produce ROS during normal respiration but can metabolize them only partially. Despite the defense system, mtDNA is particularly vulnerable because it is partially associated with the inner mitochondrial membrane [3,4].

So far, damage in mtDNA has been detected by some common methods such as Southern blotting [5] and HPLC–electrochemical detection [6]. However, one disadvantage of these techniques is that they require large quantities of mtDNA and nuclear DNA. Furthermore, because of the cost of sample preparations and the long analysis time of several hours, the techniques might not be suitable for a large-scale epidemiological study of mtDNA damage caused by oxidative stress.

To overcome these disadvantages, we propose a new methodology combining fluorescence correlation spectroscopy (FCS) with long polymerase chain reaction (LPCR). The LPCR used in the current study quantitatively amplifies the entire intact mtDNA genome alone in a small sample [7]. This technique is based on the premise that DNA

* Corresponding author. Fax: +81 238 26 3357.
E-mail address: ynomura@yz.yamagata-u.ac.jp (Y. Nomura).

[1] *Abbreviations used:* mtDNA, mitochondrial DNA; ROS, reactive oxygen species; FCS, fluorescence correlation spectroscopy; LPCR, long polymerase chain reaction; HEK-293, human embryonic kidney 293; DMEM, Dulbecco's modified Eagle's medium; PBS, phosphate-buffered saline.

0003-2697/$ - see front matter © 2006 Elsevier Inc. All rights reserved.
doi:10.1016/j.ab.2006.01.010

lesions, including those caused by oxidative damage such as strand breaks, base modification, and abasic sites, will block the progression of the polymerase, resulting in a decrease in amplification of the intact mitochondrial genome.

FCS sensitively measures fluctuations in fluorescence intensity generated by only a few fluorescent molecules diffusing in and out of an extremely tiny volume element at the subfemtoliter level in solution. The characteristics of the fluctuations are dependent on the base length and the concentration [8–10]. Thus, FCS probably detects a decrease in the LPCR product, which has the same base length as intact mtDNA. Furthermore, because of the short analysis time and the economic efficiency of the small sample volume, FCS would be advantageous for massive specimen analysis [9].

The purpose of this study was to test the feasibility of detecting mtDNA damage caused by oxidative stress using the LPCR–FCS method. After human embryonic kidney 293 (HEK-293) cells, used as test cells, were treated with different concentrations of H_2O_2 for 60 min, total cellular DNA was extracted. The mtDNA genome was amplified by LPCR and the product was confirmed with restriction enzymes. We added the fluorescent dye YOYO-1 to the LPCR medium to detect fluorescence fluctuations resulting from both the LPCR products and primer. Fluorescence autocorrelation functions were analyzed using a two-component model, and the optimal amount of template DNA was determined first. Then the dependence of the fraction of the LPCR product on H_2O_2 was evaluated.

Materials and methods

Cell culture

HEK-293 cells were grown in a 5% CO_2 humidified atmosphere at 37 °C in Dulbecco's modified Eagle's medium (DMEM) supplemented with 10% fetal bovine serum, 2×10^5 U/L penicillin G, and 200 mg/L streptomycin sulfate. The cells were routinely split every 3–4 days, and 10^6 cells were plated in 60-mm dishes 14–16 h before exposure to 0–0.4 mM H_2O_2 for 60 min [1]. Then the cells were washed once with phosphate-buffered saline (PBS) and harvested immediately by brief trypsinization (0.25%).

DNA isolation and LPCR

Using a GeneBall DNA isolation kit (TaKaRa, Japan), 30 μg of total cellular DNA was extracted from 10^6 cells. The concentration of total cellular DNA was determined by absorption at 260 nm with a SmartSpec 3000 spectrophotometer (Bio-Rad, USA). The primer nucleotide sequences were as follows: for the 16.2-kb fragment of the mitochondrial genome, the forward primer 5′-TGAG GCCAAATATCATTCTGAGGGGC-3′ and the reverse primer 5′-TTTCATCATGCGGAGATGTTGGATGG-3′ [7]; for the 17.6-kb fragment upstream of the nuclear β-globin gene (GenBank, NG_000007), the forward primer 5′-TGCACCTGCTCTGTGATTATGACTATCCCACA GTC-3′ and the reverse primer 5′-ACATGATTAGCA AAAGGGCCTAGCTTGGACTCAGA-3′. The β-globin gene encoded in the nuclear chromosome was used as a control to confirm mtDNA-specific damage.

LPCR were performed in a PC707 thermal cycler (Astec, Japan) using a TaKaRa LA Taq PCR kit as described by the manufacturer. The thermal cycle profile was as follows: initial denaturation for 1 min at 94 °C, followed by 20 cycles for mtDNA or 24 cycles for β-globin at 94 °C denaturation for 30 s and 68 °C primer extension for 15 min. A final extension at 72 °C was performed for 10 min at the completion of each profile. To confirm the LPCR product, parts of the product were digested with four restriction enzymes: *Eco*47I (TaKaRa), *Hae*III (TaKaRa), *Hga*I (New England BioLabs, USA), and *Bsp*MI (New England BioLabs). Each digest was analyzed on gel.

Fluorescence spectra of YOYO-1

The fluorescent cyanine dye YOYO-1 was purchased from Molecular Probes (USA). LPCR product–YOYO-1 complexes were made by mixing equal volumes of LPCR medium and 1 μM YOYO-1 in 10 mM Tris (pH 7.4). The mixed solution was incubated at room temperature for 30 min before use. Fluorescence spectra of YOYO-1 solution (0.5 μM) were recorded with an FP6500 fluorescence spectrophotometer (Jasco, Japan).

FCS measurement

FCS measurement was performed using a ConfoCor fluorescence correlation measurement system (Carl Zeiss Jena, Germany), as described elsewhere [11]. A sample droplet (20 μl) was set on a cover glass and was excited with approximately 10 kW/cm^2 of laser power (Ar^+) at 488 nm. The fluorescence signal was detected through a dichroic mirror (>510 nm) and a bandpass filter (515–560 nm). Measurements were conducted at room temperature.

Theoretical works on fluorescence correlation spectroscopy have been published previously by various authors [12–14]. Briefly, because fluorescence intensity fluctuates with only a few fluorescent molecules diffusing in and out of the volume element, the fluorescence intensity at time t, $I(t)$, changes into $I(t+\tau)$ τ seconds later. The fluorescence autocorrelation function is calculated from a random fluctuation of fluorescence intensity as follows:

$$G(\tau) = \frac{\langle I(t) \times I(t+\tau) \rangle}{\langle I(t) \rangle^2}. \quad (1)$$

The typical shape of an autocorrelation in Eq. (1) usually has high amplitude for time ranges shorter than approximately 1 ms and almost no amplitude for time ranges longer than approximately 1 ms. This suggests that every molecule that gives a correlation signal occupies the

volume element for a shorter time but that only a few molecules stay for a longer time. Therefore, a high amplitude lasts when large molecules stay in the volume element for a longer time because they diffuse slowly.

In the current study, the fluorescence autocorrelation function, $G(\tau)$, was fitted to a simple two-component model, where the variables were the average number of fluorescent molecules (N), the translational diffusion time of the free fast-moving component of the primer (τ_{primer}), and the translational diffusion time of the slow-moving component of the LPCR product ($\tau_{product}$), as shown in the following equation:

$$G(\tau) = 1 + \frac{1}{N}\left[\left\{\frac{1-y}{1+\frac{\tau}{\tau_{primer}}}\sqrt{\frac{1}{1+\frac{s^2\tau}{\tau_{primer}}}}\right\} + \left\{\frac{y}{1+\frac{\tau}{\tau_{product}}}\sqrt{\frac{1}{1+\frac{s^2\tau}{\tau_{product}}}}\right\}\right], \quad (2)$$

where $\tau_{primer,product} = w_0^2/4D_{primer,product}$, $s = w_o/z_o$, y is the fraction of the slow-moving component, w_o is the radius of the detection field (volume element), $2z_o$ is the field length, D_{primer} and $D_{product}$ are the translational diffusion constants of the free fast-moving product and the slow-moving product, respectively, and s is the structure parameter. The data analysis was performed using the nonlinear least-squares fitting method with the FCS ACCESS computer program (EVOTEC BioSystems, Germany). In the current study, s (0.192) was obtained previously with rhodamine 6G as the reference standard. After determining τ_{primer} and $\tau_{product}$ (see Results and discussion later), y and N were obtained from the fitting of every autocorrelation function.

The optimal amount of template DNA was determined first, and then the effect of H_2O_2 exposure on DNA damage was evaluated by changes in fraction in FCS measurement of LPCR products for mtDNA and the β-globin gene. The results were compared with those obtained by gel electrophoresis.

Frequency of DNA lesions

Assuming a random distribution of lesions, the Poisson equation (e^{-s}, where s = lesion frequency) was used to calculate the lesion frequency per genomic strand: $s = -\ln(A_d/A_o)$ = lesion frequency/strand, where A_o = the fraction of the slow component obtained from a given amount of nondamaged DNA template and A_d = the fraction of slow component of the DNA template damaged by a particular dose of H_2O_2 [15].

Densitometric analysis after gel electrophoresis

After the LPCR mixture was applied to 1% agarose gel, the gel was stained with fluorescence dye (Gelstar, TaKaRa). Then the digital image of the gel was recorded with a CCD camera (C-3040, Olympus, Japan) under UV light. The relative abundance of the LPCR product in each sample on gel was quantified by densitometric analysis using Scion Image (Scion, USA). After background subtraction, the intensities in the band of interest were divided by the highest band intensity in each gel, and the abundance was expressed as relative band intensity.

Statistical analysis

The results were analyzed for statistical significance by the unpaired Student's t test using Microcal Origin (OriginLab, USA). Values are expressed as the means and standard errors of three to five individual experiments unless stated otherwise.

Results and discussion

LPCR products labeled with YOYO-1

Using total DNA extracted from normal cells without H_2O_2 treatment, the mtDNA genome and target sequence of β-globin were amplified by LPCR. Both products were electrophoresed and appeared as single bands near 17 kbp on the gel. These were confirmed by the digestion with four restriction enzymes, demonstrating a pattern of fragment distribution identical to that expected from the GenBank data (data not shown).

In 0.5 μM YOYO-1 solution containing the mtDNA LPCR product, intense fluorescence was observed near 510 nm, as shown in Fig. 1A. YOYO-1 alone had little fluorescence at that wavelength. When interacted with the primer for mtDNA amplification, it had weak fluorescence that was one-third the fluorescence intensity of the coexistent solution of the mtDNA LPCR product. The fluorescence spectra and the intensity of the primer for the β-globin gene and of the LPCR product were identical to those for mtDNA (data not shown). Thus, the interaction between each LPCR primer and YOYO-1 also caused fluorescence.

Diffusion time of primer and LPCR products

The fluorescence autocorrelation functions of the primer for mtDNA amplification, the LPCR products for mtDNA, and the β-globin gene are shown in Fig. 1B. The function of the mtDNA LPCR product was nearly identical to that of the β-globin LPCR product due to similar base length but was largely shifted to the right compared with that of the primer. The fluorescence autocorrelation function of the primer for β-globin gene amplification was identical to that for mtDNA (data not shown). These results suggested that the LPCR product diffused much slower than the primer due to its longer length.

By fitting the autocorrelation function of the primer for mtDNA amplification to a simple one-component model, where $y = 0$ in Eq. (2), the diffusion time was obtained (Table 1). Then the fluorescence correlation functions of the mtDNA and β-globin LPCR products were fitted to

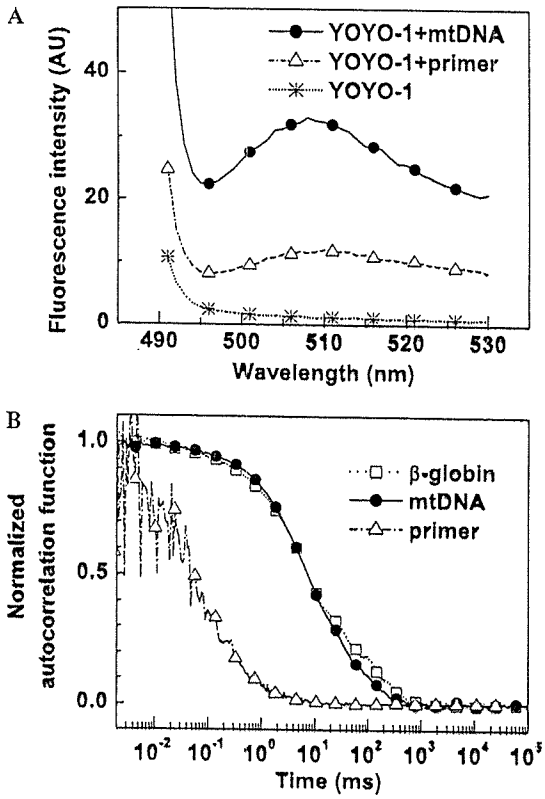

Fig. 1. (A) Fluorescence spectra (●) of 0.5 μM YOYO-1 associated with the mtDNA LPCR product, having an emission maximum at 510 nm. YOYO-1 alone (✳) had little fluorescence at the wavelength. When interacted with the primer for mtDNA amplification, it had a weak fluorescence (Δ), which was one-third the fluorescence in the solution containing the mtDNA LPCR product. (B) Typical normalized autocorrelation functions of the LPCR products of mtDNA and β-globin and the primer for mtDNA amplification.

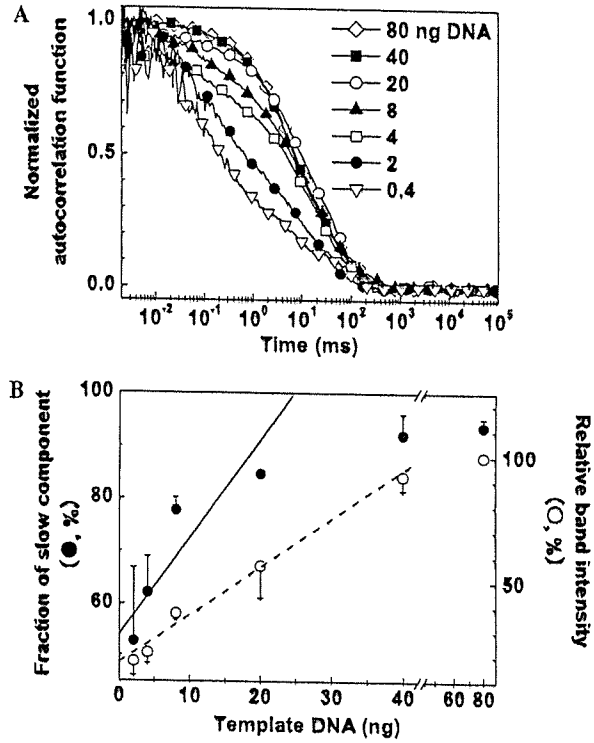

Fig. 2. (A) Changes in normalized autocorrelation functions of mtDNA LPCR products due to the amount of template DNA (0.4–80 ng). (B) Dependence of amount of template DNA on the fraction of the slow component obtained from two-component analysis of the autocorrelation function of the mtDNA LPCR product (●, means + SE) and on relative band intensity by densitometry after gel electrophoresis (○, means − SE). Regression lines are $y = 55 + 1.6x$ ($R = 0.90$) for the fraction of the slow component and $y = 17 + 1.9x$ ($R = 0.99$) for the relative band intensity (2–20 ng of total DNA).

a simple two-component model with a fast-moving component of the free primer and a slow-moving component of the LPCR product using Eq. (2). The diffusion times of the LPCR products ($\tau_{product}$) were determined by curve fitting of autocorrelation data to the two-component model and were found to be 18.2 ± 0.4 ms for mtDNA and 19.6 ± 3.3 ms for β-globin (Table 1). In the following analysis, the obtained values were considered as constant to reduce the number of free parameters.

Dependence of template DNA amount on fraction of slow component

Because the relationship between the amount of template DNA and the number of LPCR products is linear, the fraction was also expected to be dependent on the amount. As shown in Fig. 2A, the autocorrelation function of LPCR products was shifted to the left with the decrease in template DNA from 80 to 0.4 ng, showing a decrease in the slow component. When the functions were analyzed with the two-component model, the fraction of the slow component decreased consistently (Fig. 2B). At more than 20 ng, the fraction seemed to be saturated. The changes in the fraction were similar to the results obtained from densitometry (~17 kbp), although the values of the fraction in FCS were different from those of relative band intensities, which were normalized with the band intensity of 80 ng of template DNA. The results suggest that we can detect the decrease in LPCR product, caused by oxidative stress, if up to 20 ng of template DNA is used under the current conditions of LPCR.

Table 1
Diffusion time of the primer (τ_{primer}) for mtDNA amplification, LPCR products ($\tau_{product}$) for mtDNA, and β-globin

	Primer	mtDNA	β-Globin
Diffusion time (ms)	0.21 ± 0.03	18.2 ± 0.4	19.6 ± 3.3
Number of samples	5	4	3

Note. Values are expressed as means and standard errors.

Effect of H_2O_2 on fraction of slow component

Cells were treated with various concentrations of H_2O_2 up to 1 mM for 1 h. Just after exposure to 1 mM, cells detached from culture dishes. Under conditions up to 0.4 mM, cells remained attached. When cells were treated with 0.4 mM H_2O_2, cell growth was suppressed 2 days after the treatment, probably due to apoptosis [1].